Effect of ions on sulfuric acid-water binary particle formation: 2. Experimental data and comparison with QC-normalized classical nucleation theory

J. Duplissy[1,2], J. Merikanto[3], A. Franchin[2], G. Tsagkogeorgas[4], J. Kangasluoma[2], D. Wimmer[2,5], H. Vuollekoski[2], S. Schobesberger[2,6], K. Lehtipalo[2], R. C. Flagan[7], D. Brus[3], N. M. Donahue[8], H. Vehkamäki[2], J. Almeida[5,9], A. Amorim[10], P. Barmet[11,12], F. Bianchi[11,13], M. Breitenlechner[14], E. M. Dunne[15,16], R. Guida[9], H. Henschel[2], H. Junninen[2], J. Kirkby[5,9], A. Kürten[5], A. Kupc[17], A. Määttänen[18], V. Makhmutov[19], S. Mathot[9], T. Nieminen[1], A. Onnela[9], A. P. Praplan[2], F. Riccobono[11], L. Rondo[5], G. Steiner[2,14,17], A. Tome[10], H. Walther[11], U. Baltensperger[11], K. S. Carslaw[15], J. Dommen[11], A. Hansel[14,20], T. Petäjä[2], M. Sipilä[2], F. Stratmann[4], A. Vrtala[17], P. E. Wagner[17], D. R. Worsnop[2,21], J. Curtius[5], and M. Kulmala[2]

[1]Helsinki Institute of Physics, University of Helsinki, Helsinki, Finland, [2]Department of Physics, University of Helsinki, Helsinki, Finland, [3]Finnish Meteorological Institute, Helsinki, Finland, [4]Leibniz Institute for Tropospheric Research, Leipzig, Germany, [5]Institute for Atmospheric and Environmental Sciences, Goethe University Frankfurt, Frankfurt am Main, Germany, [6]Now at Department of Atmospheric Sciences, University of Washington, Seattle, Washington, USA, [7]Division of Chemistry and Chemical Engineering, California Institute of Technology, Pasadena, California, USA, [8]Center for Atmospheric Particle Studies, Carnegie Mellon University, Pittsburgh, Pennsylvania, USA, [9]PH Department, CERN, Geneva, Switzerland, [10]CENTRA-SIM, F.C.U. Lisboa and U. Beira Interior, Covilhã, Portugal, [11]Laboratory of Atmospheric Chemistry, Paul Scherrer Institute, Villigen, Switzerland, [12]Now at Department Construction, Traffic and Environment, Canton of Aargau, Aarau, Switzerland, [13]Institute for Atmospheric and Climate Science, ETH Zurich, Zurich, Switzerland, [14]Institute for Ion and Applied Physics, University of Innsbruck, Innsbruck, Austria, [15]School of Earth and Environment, University of Leeds, Leeds, UK, [16]Atmospheric Research Centre of Eastern Finland, Finnish Meteorological Institute, Kuopio, Finland, [17]Aerosol Physics and Environmental Physics, University of Vienna, Vienna, Austria, [18]Université Versailles St-Quentin; Sorbonne Universités, UPMC Univ. Paris 06; CNRS/INSU, LATMOS-IPSL, Guyancourt, France, [19]Solar and Cosmic Ray Research Laboratory, Lebedev Physical Institute, Moscow, Russia, [20]Ionicon Analytik GmbH, Innsbruck, Austria, [21]Aerodyne Research Inc., Billerica, Massachusetts, USA

Abstract We report comprehensive, demonstrably contaminant-free measurements of binary particle formation rates by sulfuric acid and water for neutral and ion-induced pathways conducted in the European Organization for Nuclear Research Cosmics Leaving Outdoor Droplets chamber. The recently developed Atmospheric Pressure interface-time of flight-mass spectrometer was used to detect contaminants in charged clusters and to identify runs free of any contaminants. Four parameters were varied to cover ambient conditions: sulfuric acid concentration (10^5 to 10^9 mol cm^{-3}), relative humidity (11% to 58%), temperature (207 K to 299 K), and total ion concentration (0 to 6800 ions cm^{-3}). Formation rates were directly measured with novel instruments at sizes close to the critical cluster size (mobility size of 1.3 nm to 3.2 nm). We compare our results with predictions from Classical Nucleation Theory normalized by Quantum Chemical calculation (QC-normalized CNT), which is described in a companion paper. The formation rates predicted by the QC-normalized CNT were extended from critical cluster sizes to measured sizes using the UHMA2 sectional particle microphysics model. Our results show, for the first time, good agreement between predicted and measured particle formation rates for the binary (neutral and ion-induced) sulfuric acid-water system. Formation rates increase with RH, sulfuric acid, and ion concentrations and decrease with temperature at fixed RH and sulfuric acid concentration. Under atmospheric conditions, neutral particle formation dominates at low temperatures, while ion-induced particle formation dominates at higher temperatures. The good agreement between the theory and our comprehensive data set gives confidence in using the QC-normalized CNT as a powerful tool to study neutral and ion-induced binary particle formation in atmospheric modeling.

1. Introduction

The majority of aerosol particles in Earth's atmosphere are estimated to originate from gas-to-particle transformation [*Merikanto et al.*, 2009]. Sulfuric acid has long been thought to be one of the main species initiating particle formation in the atmosphere due to its low vapor pressure and its strong affinity for water. Recent findings show that trace levels (a few parts per trillion (ppt)) of other species, e.g., amines [*Murphy et al.*, 2007;

Kurten et al., 2008; *Kürten et al.*, 2014; *Almeida et al.*, 2013; *Bianchi et al.*, 2014], oxidized organics [*Kulmala et al.*, 2004; *Zhang et al.*, 2009; *Metzger et al.*, 2010; *Riccobono et al.*, 2012; *Schobesberger et al.*, 2013; *Ehn et al.*, 2014; *Riccobono et al.*, 2014], and ammonia [*Ziereis and Arnold*, 1986; *Ball et al.*, 1999; *Kirkby et al.*, 2011; *Schobesberger et al.*, 2015] likely contribute to particle formation in the lower troposphere [*Kulmala et al.*, 1998; *Zhang et al.*, 2012; *Kulmala et al.*, 2013; *Berndt et al.*, 2014]. Observations in the atmospheric boundary layer suggest that new particle formation takes place mainly through a neutral pathway, with an ion-induced contribution of only around 10% [*Laakso et al.*, 2007; *Manninen et al.*, 2009].

In the upper troposphere and lower stratosphere, where the temperature is low, binary water-sulfuric acid nucleation processes may be important sources of new particles. At these altitudes, particle formation can also be significantly enhanced by species such as ammonia [*Ball et al.*, 1999; *Kirkby et al.*, 2011]. The binary formation of new particles that are initially around 1 nm in diameter can also be significantly enhanced by the presence of ions [*Raes and Janssens*, 1986; *Lovejoy et al.*, 2004; *Kirkby et al.*, 2011] that mainly derive from cosmic rays. These nanometer-sized particles can subsequently grow to 50–100 nm, sufficiently large to act as cloud condensation nuclei (CCN). Therefore, changes in atmospheric particle formation by ions could potentially affect CCN concentrations and cloud properties.

The impact of solar variation on climate has been widely discussed [e.g., *Kirkby*, 2007; *Gray et al.*, 2010]. Solar activity variation modulates the cosmic ray flux entering the atmosphere and could potentially modulate cloud properties through an ion-particle formation-particle growth-CCN link. The CLOUD (Cosmics Leaving OUtdoor Droplets) project at European Organization for Nuclear Research (CERN) investigates the effects of galactic cosmic rays on aerosol and cloud formation, and hence on climate. Here we report neutral and ion-enhanced water-sulfuric acid particle formation rates (referred hereafter to as the binary process) measured during the CLOUD5 campaign in 2011; we compare the measurements with the QC-normalized Classical Nucleation Theory (CNT) [*Merikanto et al.*, 2016]. In a companion paper [*Merikanto et al.*, 2016] (hereafter referred to as Paper 1), we give a full representation of this most recent version of CNT. The measurements were carried out at temperatures, sulfuric acid concentrations, relative humidities, and ion concentrations spanning tropospheric conditions. Throughout both papers, we use the term "particle formation" generally to describe the generation of new particles from the vapor phase and use the term "nucleation," which is often used synonymously, only when this process involves the crossing of a free-energy barrier, at the top of which is located at the critical cluster size.

Besides its atmospheric significance, knowledge of the binary process is vital for understanding processes involving more than two components and atmospheric particle formation as a whole. Despite extensive research over many decades, measurements of particle formation lack the precision and coverage of relevant tropospheric conditions to enable quantitative model evaluation; moreover, they suffer from inadequate control over impurities. As a result, theoretical models describing the process have yet to be fully validated. During CLOUD5, we were able to measure the particle formation rate at very small particle sizes while simultaneously monitoring the cluster composition. The CLOUD chamber experiments use the state-of-art instruments while ensuring ultraclean conditions [*Kirkby et al.*, 2011; *Bianchi et al.*, 2012; *Praplan et al.*, 2012; *Schnitzhofer et al.*, 2014; *Almeida et al.*, 2013]. This unique facility, combined with the broader CERN facilities and expertise, has made it possible to run experiments with extremely low levels of impurities, while spanning the extreme temperatures encountered in different regions of the atmosphere, thereby providing data that fill this critical gap in our understanding.

1.1. Brief Review of Water-Sulfuric Acid Particle Formation Experiments

The search for an accurate understanding of binary water-sulfuric acid particle formation has a long history, which is briefly reviewed here. The first quantitative laboratory experiments were made by *Reiss et al.* [1976] in a piston cloud chamber; these studies were followed by reactor experiments conducted by *Boulaud et al.* [1977] and experiments in an upward thermal diffusion cloud chamber by *Mirabel and Clavelin* [1978]. *Cox* [1973] and *Friend et al.* [1980] conducted flow reactor studies of gas-to-particle conversion involving sulfuric acid produced during photooxidation of sulfur dioxide (SO_2). These studies demonstrated the likely atmospheric significance of sulfuric acid-water particle formation originally suggested by binary CNT [e.g., *Reiss*, 1950; *Mirabel and Katz*, 1974; *Shugard et al.*, 1974], but the thermodynamic data and instrumentation available in that era limited the rigor with which experimental and theoretical results could be compared.

Nonetheless, the experimental results stimulated advances in the theoretical work. CNT was updated to include the effects of hydrate formation due to the strong binding affinity of sulfuric acid to water [e.g., *Heist and Reiss*, 1974; *Shugard and Reiss*, 1976; *Jaecker-Voirol and Mirabel*, 1988; *Lazaridis et al.*, 1991; *Kulmala et al.*, 1991]. Accurate quantitative theoretical prediction of nucleation rates requires thermodynamic data on properties like surface tension and equilibrium vapor pressure over the temperature and pressure range of the experiments, but the available data were highly uncertain. For example, in the late 1970s the suggested values of equilibrium vapor pressure for pure sulfuric acid ranged from about 1.3×10^{-9} atm to 5×10^{-7} atm at 298 K [*Gmitro and Vermeulen*, 1964; *Doyle*, 1961; *Kiang and Stauffer*, 1973], thus introducing a large uncertainty into theoretical predictions. The first measurements of the equilibrium vapor pressure of sulfuric acid were conducted by *Roedel* [1979], who found a value of 3.29×10^{-9} atm at 296 K. Later measurement results by *Ayers et al.* [1980] were close to those of *Roedel* [1979] (lower by a factor of 3), even though the latter measurements were performed at much higher temperatures (338–445 K). Measurements of the equilibrium vapor pressure of sulfuric acid at 300–343 K by *Marti et al.* [1997] generally agree with the predictions of *Ayers et al.* [1980], although the observed vapor pressure exceeded that predicted for the more dilute solutions. The experimental equilibrium vapor pressure expression of *Ayers et al.* [1980], later extrapolated to atmospheric temperatures by *Kulmala and Laaksonen* [1990], is used today in binary nucleation calculations [e.g., *Vehkamaki et al.*, 2002]. We shall also employ that expression in this study.

Wyslouzil et al. [1991] published the first temperature-dependent nucleation rate data (nucleation temperatures, $T_{nuc} = 293.3$, 298.3, and 303.3 K) for the sulfuric acid-water system. Their measurements differed from the theoretical Jaecker-Voirol-Mirabel nucleation rates by a factor varying between 10^{-11} and 10^{12}. On the other hand, in flow-tube experiments using Titrisol® solutions of sulfuric acid in water, *Viisanen et al.* [1997] obtained agreement between the measured rates and the hydrate-corrected and thermodynamically consistent version of CNT by *Wilemski* [1987]. The sulfuric acid concentration was not directly measured in either of these studies; instead, it was calculated from mass balance considerations or from the saturation vapor pressure or molality of a weak sulfuric acid solution.

Using a selected ion chemical ionization mass spectrometer [*Eisele and Tanner*, 1993], *Ball et al.* [1999] performed the first experiments (at 295 K) in which the sulfuric acid vapor concentration was directly measured. They also detected freshly nucleated particles down to 3 nm (>50% detection efficiency) with an Ultrafine Condensation Nucleus Counter [*Stolzenburg and McMurry*, 1991], thereby providing the most comprehensive data set on sulfuric acid-water nucleation at that time. Both the measurements of *Ball et al.* [1999] and those of *Viisanen et al.* [1997] are in reasonable agreement with predictions made using the rigorous theoretical approach of *Noppel et al.* [2002] (see Paper 1). Hence, this theoretical approach was used in the widely applied nucleation parameterization by *Vehkamaki et al.* [2002]. Binary nucleation data for the sulfuric acid-water system can be found also in the work of *Zhang et al.* [2004], who also used an ultrafine condensation particle counter and a mass spectrometer to detect and characterize forming particles, although their work was primarily focused on the enhancement of nucleation by organic acids. Both *Ball et al.* [1999] and *Zhang et al.* [2004] used pure liquid sulfuric acid as a source of sulfuric acid vapor; the results of these two studies agree closely.

During the last decade, most experimental studies of the neutral binary system focused on particle formation under atmospheric boundary layer conditions, and, except for the CLOUD continuously stirred tank reactor (CSTR) experiments, relied on flow-tube techniques. These experiments have produced gas phase sulfuric acid by a photooxidation of SO_2 [e.g., *Berndt et al.*, 2005; *Benson et al.*, 2008; *Young et al.*, 2008; *Sipila et al.*, 2010, *Kirkby et al.*, 2011] or by evaporation from dilute solutions [*Brus et al.*, 2010, 2011] or neat sulfuric acid [*Zollner et al.*, 2012]. Binary homogeneous nucleation results from these studies were often in stark disagreement with the parameterization of *Vehkamaki et al.* [2002], but the source of sulfuric acid vapor also appeared to affect the experimental outcomes. Two experimental limitations apply to these experiments: contamination by minute but significant levels of trace gases, and a significant difference between the extremely small critical cluster size and the minimum measurable particle size. Until very recently, no measurement techniques existed to address either limitation.

Even though these recent studies were executed with care and purported to address binary nucleation, most were, to some extent, burdened with *ppt* level contamination by base impurities like ammonia and amines.

These trace-level contaminants were shown to arise from various sources such as the water used for carrier gas humidification, the carrier gas itself, or simply surfaces in the experimental system [e.g., *Benson et al.*, 2011; *Brus et al.*, 2011; *Kirkby et al.*, 2011]. Only recently have advances in analytical techniques like mass spectrometry [e.g., *Ehn et al.*, 2010; *Junninen et al.*, 2010; *Zhao et al.*, 2010; *Jokinen et al.*, 2012; *Schobesberger et al.*, 2015] and ion chromatography [*Praplan et al.*, 2012] made it possible to monitor these low-level impurities in the formed molecular clusters and in the gas phase. The first experiments at CLOUD [*Duplissy et al.*, 2010; *Kirkby et al.*, 2011] were designed to address binary nucleation alone, but only after new measurement methods were employed, trace contamination by ammonia was detected and subsequently reduced.

Newly developed detectors have also pushed size cutoffs close to the critical cluster size [*Iida et al.*, 2009]. These include the Particle Size Magnifier (PSM) [*Vanhanen et al.*, 2011], diethylene-glycol condensation particle counters (DEG-CPC) [*Wimmer et al.*, 2013], and the pulse height analyzer ultrafine condensation particle counter (PHA-UCPC) [*O'Dowd et al.*, 2004]. These detectors have achieved sufficient sensitivity to directly count particles below 3 nm in diameter, contributing to uncovering the reason behind the discrepancies among the sulfuric acid power dependencies of formation rates in the previous studies, even though the contamination problems remained [*Sipila et al.*, 2010].

Discrepancies between different measurements have been shown to arise from contamination and depletion of sulfuric acid in the flow tube, hampering the growth of formed particles to observable sizes before being lost to the walls, together with the fact that different instruments have different cutoff sizes, and transmission curves that are also not step functions at the cutoff diameter. Reviews and discussion of the results of experimental studies performed to date can be found in the existing literature [e.g., *Brus et al.*, 2010; *Zollner et al.*, 2012; and *Zhang et al.*, 2012]. *Ehrhart and Curtius* [2013] have shown that for experimental conditions, where growth rates are slow compared to the loss rates of clusters to either the reactor walls or larger aerosol particles, derived nucleation rates, and their dependencies on the H_2SO_4 concentration are influenced by the loss processes. This finding suggests another reason for diverging experimental results as the loss processes differ from experiment to experiment.

1.2. Brief Review of the Effect of Ions on Particle Formation Studies

The impact of ionizing radiation on particle formation was first studied in the late nineteenth century by Wilson, who irradiated an expansion chamber with X-rays and radioactive materials, e.g., uranium, and observed that the ions induced droplet formation [*Wilson*, 1895, 1899]. Later experiments [*Metnieks and Pollak*, 1959; *Megaw and Wiffen*, 1961] explored the link between the strength of radiation and the concentrations of the resulting particles. *Vohra et al.* [1984] observed enhanced particulate sulfate production when radon was injected into a mixture of SO_2, O_2, and C_2H_4. The effect of UV and gamma rays on particle formation in a gaseous mixture of SO_2 and NO_2 was investigated by *Raes et al.* [1985]. *Mäkelä et al.* [1995] performed experiments in which humid air containing SO_2 was irradiated and showed that the bimodal size distribution predicted by the ion-induced CNT was qualitatively correct. *Kim et al.* [1997] quantitatively compared ion-induced and neutral binary nucleation at various levels of SO_2 as well as water vapor and various irradiation times by α-rays and concluded that the contribution of ion-induced to total nucleation was lowered when the concentration of SO_2 was increased.

Lovejoy et al. [2004] measured the thermodynamics of small cluster ions containing sulfuric acid and concluded that, while ion-induced particle formation cannot explain observations in the boundary layer, the process can be significant in the middle and upper troposphere. In a study of particle nucleation at atmospherically relevant concentrations of SO_2, O_3, and water vapor, *Svensmark et al.* [2007] reported that the production of particles under these conditions is proportional to the negative ion density and hypothesized that atmospheric ions continuously generate a reservoir of ready-to-grow thermodynamically stable clusters. In a pilot CLOUD chamber experiment, *Duplissy et al.* [2010] investigated the effect of ionizing particle radiation on aerosol formation from trace H_2SO_4 vapor ($\leq 10^6 \, mol \, cm^{-3}$). They concluded that ion-induced nucleation or ion-ion recombination was a source of particles. In later CLOUD1-CLOUD3 measurements, *Kirkby et al.* [2011] reported a clear enhancement in binary particle formation rates due to ions at 248 K. The CLOUD5 data presented here are verifiably from the binary H_2SO_4/H_2O system and cover a wide range of tropospheric conditions. We also show that Classical Nucleation Theory normalized by Quantum Chemical calculation (QC-normalized CNT), described in Paper 1, can describe the process with remarkable accuracy.
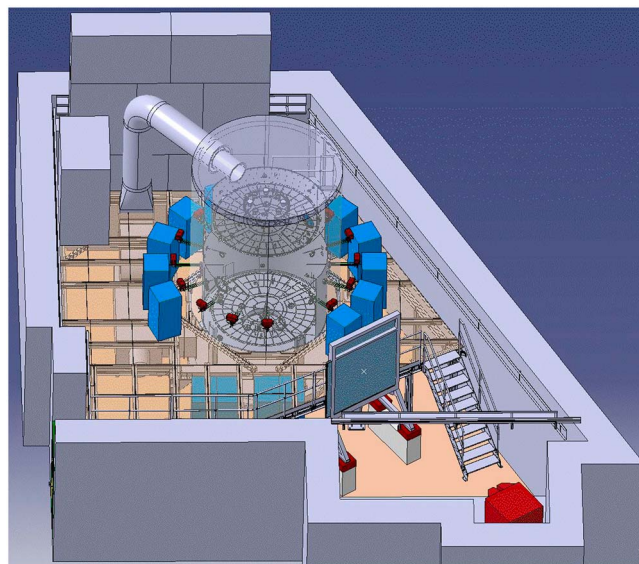
2. Methods

2.1. CLOUD Chamber

Figure 1. An illustration of CLOUD in the T11 experimental zone at the CERN PS. The defocused particle beam exits a dipole magnet (bottom right), crosses the aluminum hodoscope counter (middle), and then traverses the 3 m diameter CLOUD chamber before being stopped by the concrete wall (top left). The instruments (blue boxes) analyze the contents of the chamber via sampling probes. Air at a precisely controlled temperature circulates between the chamber and the thermal housing. Both the thermal housing and the chamber are shown partly transparent, revealing the circular field cage electrodes that create the clearing field for the removal of ions (bottom and top part of the chamber).

Here we describe the CLOUD chamber, focusing on the setup during the CLOUD5 experiment. A short general description of the CLOUD chamber can be found in the supporting information of *Kirkby et al.* [2011]. The CLOUD chamber is installed on the T11 beam line in the East Hall at the CERN Proton Synchrotron (PS) (Figure 1). Because the CLOUD chamber is not underground, it is continuously exposed to galactic cosmic rays (GCR). In addition to galactic cosmic rays, the chamber can be exposed to a 3.5 GeV/c secondary pion beam (π beam) from the CERN PS. This beam corresponds to the characteristic energies and ionization rates of cosmic ray muons in the lower troposphere. The CERN PS π beam is typically highly focused, but for the CLOUD experiment it is defocused to a transverse size of about $150 \times 150 \, cm^2$ across the chamber. The beam intensity can be adjusted to span the natural range of equilibrium ion-pair (i.p.)

concentrations from ground level (about 200 i.p. cm^{-3}) up to stratospheric values (about 6000 i.p. cm^{-3}) [*Duplissy et al.*, 2010]. Any intermediate setting between these minimum and maximum levels can be achieved by adjusting the beam collimators or the frequency of the π-beam cycle. Even though galactic cosmic rays are always present, the ion-pair concentration can also be reduced down to a few i.p. cm^{-3} by applying a high-voltage clearing electric field inside the chamber. To achieve this, a high-voltage field cage comprising two electrodes is installed inside the chamber. Voltages in a range of ± 30 kV can be applied to the two electrodes. When high voltage is applied, these electrodes create an internal electric field of up to 20 kV m^{-1}, thus removing all ions within a second (which is much shorter than the typical interval between collisions of relevant molecules, ~1000 s for a sulfuric acid concentration of $10^7 \, cm^{-3}$).

A technical schematic of the CLOUD chamber is shown in Figure 2. The chamber is a 3 m diameter ~3.5 m high electropolished, 316 L stainless steel cylinder ($26.1 \, m^3$). Grounded stainless steel enables much better control over the concentration of ions than is possible with a traditional Teflon chamber, where most ions would be stripped away and charges accumulating on the Teflon surfaces produce uncontrollable electric fields. The stainless steel also allows a higher standard of cleanliness. Two stainless steel fans are mounted inside the chamber at the bottom and the top; these are magnetically coupled to flexible drives connected to motors located outside the chamber. The fans run in counter flow to achieve efficient turbulent mixing of the gases and the ions in the chamber [*Voigtlaeander et al.*, 2012].

The chamber is surrounded by an insulated thermal housing and has been designed to achieve a high standard of temperature stability. The CLOUD chamber temperature is controlled by precisely regulating the temperature of air circulating in the space between the chamber and the thermal housing (see Figures 1 and 2). Experimental runs can presently be performed at temperatures between 207 K and 310 K, and they are stable to within 0.1 K. During chamber cleaning, the temperature can be raised to 373 K. Forty temperature sensors monitor the temperature of the chamber's external wall. A string of 5 PT100 temperature sensors is placed at midplane level inside the chamber, at distances of 0.05, 0.2, 0.4, 0.8, and 1.2 m from the chamber wall. The value at 1.2 m distance is used as the chamber's reference temperature and is symbolized with a "T" in Figure 2.
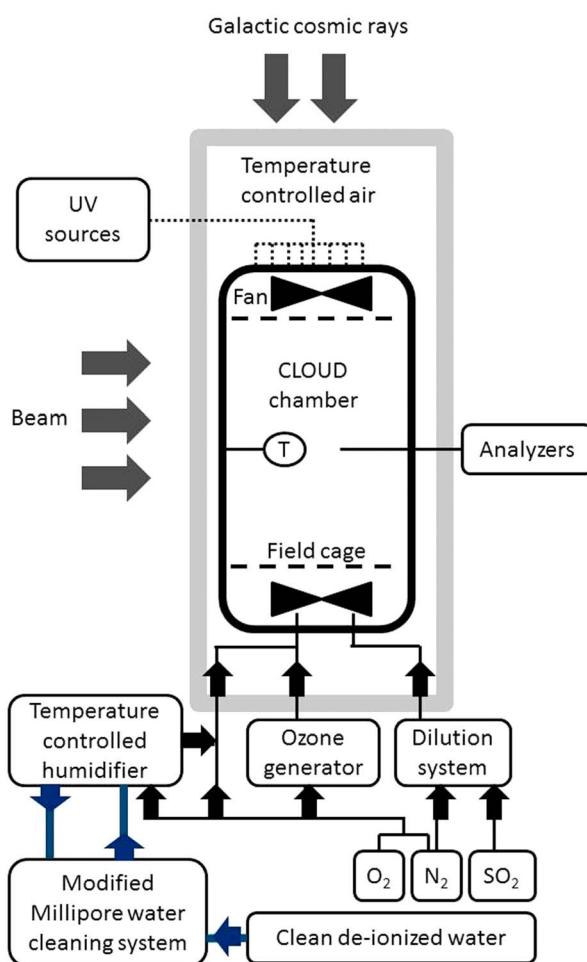
Figure 2. CLOUD experiment schematic. Clean deionized water is introduced to a modified Millipore water cleaning system where it is recirculated and filtered continuously. Water vapor is added to purified dry air via a Nafion membrane in the humidifier. All different gases (SO_2, O_3, and humid air) have their own line and arrive at the bottom of the chamber, just below a mixing fan. Inside the chamber, two fans, one at the bottom and one at the top, work in counter flow to ensure uniform mixing of the gases. The inside of the chamber can be irradiated by UV light introduced from the top of the chamber. Ions are produced by galactic cosmic rays and additionally by using the CERN PS beam. A clearing field can be switched on to remove the ions when needed. The chamber is surrounded by a thermal housing. Temperature-controlled air is circulated around the chamber to maintain a constant temperature inside the chamber.

CLOUD is filled with ultrapure synthetic, humidified air. Ultrapure dry air is obtained from the evaporation of cryogenic liquid N_2 (Carbagas, 99.9999%) and liquid O_2 (Carbagas 99.998%), which are mixed in a 79:21 ratio. A portion of the flow passes through a Nafion humidifier and is then mixed with the ultrapure dry air. Deionized water is continuously recirculated in an adapted Millipore Super-Q system, which includes one active carbon cartridge (Millipore CDFC02203), two ion-exchange cartridges (Millipore CPMB02202), one active organic cartridge (Millipore CPEX02201), one 0.22 μm particle filter (Millipore CVDI01TPE), and ultraviolet radiation. The recirculated clean water is passed through a temperature-controlled Nafion humidifier (Perma Pure, FC150-480-10SSK). By precisely adjusting the temperature and air flow through the Nafion humidifier, the relative humidity in the CLOUD chamber can be adjusted and controlled. Great care has been taken to avoid any water condensation prior to the introduction of humid air into the chamber by heating the tube in which the gases are mixed. The humid air is then cooled down to the chamber's internal temperature prior to entering the chamber.

Trace gases are also controlled with care. Ozone is created in a separate glass flow tube by UV photolysis of the cryogenic O_2 using a UV lamp (SterilAir, 30W). The ozone concentration is regulated by adjusting the flow of oxygen being irradiated. It is then mixed with the main flow of air upstream of the point where that flow enters the chamber (Figure 2). Trace amounts of SO_2 are added from gas cylinders (Carbagas, 99.95%) with pressurized N_2 as the carrier. The input concentration of SO_2 is precisely regulated by the use of three mass flow controllers (MFC) and valves. The chamber and gas supply were designed to achieve and sustain the highest standards of cleanliness. All MFC, tubes, and connections are pure stainless steel without any organic components.

The contents of the chamber can be irradiated with UV light of adjustable intensity (0 to 124 mW m^{-2}) with wavelengths in the range 250–750 nm. The UV is produced by four Hamamatsu LC8 UV light sources (200 W Hg-Xe lamp) and is introduced via 239 optical fiber vacuum feedthroughs installed on top of the chamber [Kupc et al., 2011]. Because the lamps and all electronics are outside the chamber, this system produces negligible heat load. The adjustable UV irradiation stimulates further reactions; in the case of CLOUD5, the oxidation of SO_2 to H_2SO_4 is triggered by the production of OH radicals, formed after photolysis of O_3 in the presence of H_2O. By varying the light intensity, the H_2SO_4 production rate can be adjusted.

Instruments can sample chamber air from 14 electropolished stainless steel sampling probes placed around the chamber, in the midplane level (where the clearing field is at 0 V). The probes are 0.75 m long and project 0.3 m into the chamber. Probe internal diameters of 10.4 or 22.35 mm are used, depending on the flow rate of sampling air, to avoid turbulence and to minimize losses. Actively cooled copper linings maintained at the chamber temperature have been brazed around the portions of probes extending out of the chamber to keep the temperature of the sampled air close to the chamber temperature. The contents of the chamber are continuously analyzed by instruments connected to the sampling probes. The total gas flow (including N_2, O_2, H_2O, O_3, and SO_2,) entering the chamber is kept constant at 140 L min^{-1}. The total inflow to the chamber is larger than the outflow to the instruments. An adjustable exhaust flow is used to maintain the chamber pressure a few hPa above ambient pressure. The high volume of the chamber allows experiments to last for several hours with a flushing time scale of 3 h in the case of CLOUD5 experiments. The mixing time scale of the chamber is short compared to the flushing time scale, and both input and output flows are kept constant, and thus the chamber operates as a CSTR. Well-defined start times ($t = 0$) for experiments are established by turning on UV illumination or by turning off (or on) the ion clearing field, or by opening the π beam.

Prior to the start of the campaign, the chamber was actively cleaned in three steps. First, high-pressure ultrapure water was used to rinse the inside wall of the chamber; second, the temperature was increased to 373 K while the chamber was flushed with wet ultrapure air for several days; and third, the chamber was continuously flushed with high concentrations of ozone (ppm level) for 1 day.

2.2. Analyzers

The CLOUD experiment is equipped with state-of-the-art ion, particle and trace gas detectors for a thorough investigation of the first steps of particle formation and growth. The instruments used during CLOUD5 and their application in this study are briefly presented below.

2.2.1. Galactic Cosmic Ray Flux and π-Beam Monitors

Galactic cosmic ray (GCR) fluxes are monitored by a GCR detector situated nearby but outside of the beam area. The GCR instrument consists of 120 gas-discharge cylindrical Geiger counters arranged in 12 blocks, each of which contains 10 counters. All blocks are located on a platform ~1 × 1 m in size. It provides, with 500 ms integration time, a continuous detection of total charged particle abundance that consists of galactic cosmic rays (secondary component), natural radioactivity, and any scattered particles produced by the particle PS beam. The π-beam intensity is measured by two independent scintillation counters. A plastic scintillation counter of 140 × 20 cm is placed immediately at the exit of the beam. A plastic scintillation counter hodoscope of overall size 180 × 180 cm, comprising nine vertical counters followed by nine horizontal counters all of the size of 180 × 20 cm, provides the vertical and horizontal beam intensity profile with a time resolution that can be adjusted from 25 ms up to few seconds [*Mizin et al.*, 2011]. It is located 5.4 m from the beam exit in front of the CLOUD chamber (see Figure 1). The beam intensity measurements from the two scintillation detectors agree well with each other. A comparison of the data from the two scintillation counters and the ion production rate as a function of beam intensity, temperature, and humidity is presented in *Franchin et al.* [2015].

2.2.2. Ion Composition and Size Distribution Detectors

The concentration and size distribution of ions in the chamber that have electric mobility diameters ranging from 0.8 nm to 42 nm were measured with one Neutral cluster and two Air Ion Spectrometers (NAIS), one for positive ions and one for negative ions. The NAIS is a differential mobility analyzer in which sampled ions are collected simultaneously on 21 electrometer rings to produce parallel measurements of 21 electrical mobility fractions for each polarity (see *Manninen et al.* [2010] for details). An Atmospheric Pressure interface-Time Of Flight-Mass Spectrometer (APi-TOF-MS) measured the ion cluster mass spectra in the chamber. The instrument consists of a sampling inlet, Atmospheric Pressure interface (APi), and a high-resolution time-of-flight mass spectrometer. Chemical species are identified from their exact mass signatures and isotopic fractions, for positive and negative ions up to 2000 Th [*Junninen et al.*, 2010; *Ehn et al.*, 2010; *Schobesberger et al.*, 2013]. During CLOUD5, the APi-TOF-MS usually operated in the negative mode, where sulfuric acid ions can be detected. The APi-TOF-MS is a key instrument in this study as it can differentiate clusters produced by pure binary processes, i.e., containing only sulfuric acid and water, from clusters also containing other molecular species. Even though not all trace gas contaminations could be detected directly in the gas phase, the APi-TOF-MS is sufficiently sensitive to determine if additional species are participating in the initial cluster formation, albeit with the limitation that it can only measure charged molecular clusters. The

Table 1. Estimated Cutoff Size Ranges of the Different Particle Counters Over the Course of the Campaign[a]

Particle Counter	Estimated Cutoff Size
PSMa	~1.3 ~ 1.6 nm
PSMb	~1.6 ~ 1.8 nm
DEGa	~2 nm
DEGb	~2.7 nm
UCPC	~3.2 nm

[a]The cutoff size corresponds to the mobility diameter at which 50% of the particles are detected, including sampling line losses. See *Wimmer et al.* [2015] for the details.

separation into "pure H_2SO_4/H_2O binary" or "contaminated" particle formation classes in this study is based on the molecular identification of the clustered species using the APi-TOF-MS. This procedure is further discussed in section 3.1.

2.2.3. Particle Number Concentration and Size Distribution Measurements

The particle formation rate was determined by a series of particle counters with cutoff sizes ≤ 3.2 nm. The counters enabled simultaneous constraints on formation and growth rates, which is essential to determine accurate values for both of the rates [*Kürten et al.*, 2015]. They included one Ultrafine Condensation Particle Counter (UCPC, TSI 3776) with a cutoff size of 3.2 nm mobility diameter, two Particle Size Magnifiers (PSM, Airmodus A09), and two Diethylene-Glycol Condensation Particle Counters (DEG-CPCs). The PSMs and DEG-CPCs are state-of-the-art particle counters with adjustable particle size detection thresholds, using diethylene-glycol as a working fluid. The total inlet flow rate of the PSM is 2.5 L min^{-1}. It produces supersaturation by mixing the ambient-temperature aerosol flow with a flow of heated particle-free air from a DEG saturator; varying the saturator flow rate rapidly changes the supersaturation and determines the PSM cutoff size [*Vanhanen et al.*, 2011]. The DEG-CPC works in a similar way as the PSM, except that instead of having a turbulent mixing in the DEG section, it employs a continuous laminar flow [*Wimmer et al.*, 2013]. The temperature of the saturator flow is changed to alter the cutoff size. The two PSMs and the two DEG-CPCs were set to different fixed cutoff sizes, which have been determined in the laboratory using ammonium sulfate particles [*Wimmer et al.*, 2013, *Kangasluoma et al.*, 2013]. As the temperature of sampled air influences the cutoff size of the instrument [*Wimmer et al.*, 2015], the instrumental settings were adjusted according to the sampling air temperatures (varying from 207 to 298 K) to keep an approximately fixed cutoff size through the entire campaign. An estimation of the mobility diameter cutoff sizes for each detector used during CLOUD5 is summarized in Table 1.

The particle size distribution in the ~7–120 nm range was measured with a scanning mobility particle spectrometer (SMPS). The SMPS consisted of a neutralizer (Krypton 85) and a short Differential Mobility Analyzer (short DMA) coupled to a CPC (TSI 3786). The neutralizer and the short DMA were in a temperature-controlled rack, matching the chamber temperature down to 248 K, and kept at this temperature for measurements at lower temperatures, whereas the CPC 3786 was at ambient temperature. The SMPS data were used to calculate the coagulation sink, making it possible to calculate loss-corrected particle formation rates in different size ranges.

To minimize the losses through the sampling probes and the consequent loss correction to apply to the data, core-sampling probes were used for all the particle instruments described above. The instruments drew samples via the core-sampling probe from the middle of the sample flow at an isokinetic rate, optimizing the sampling efficiency of the sampling probe, typically with a core flow of 2.5 L min^{-1} and a bypass flow of 5 L min^{-1} [*Wimmer et al.*, 2015].

2.2.4. Gas Phase Measurements

Sulfuric acid was measured with a Chemical Ionization Mass Spectrometer (CIMS) from THS Instruments (THS Instruments LLC, USA). A detailed description of the instrument, its principle of operation, and its calibration can be found elsewhere [*Eisele and Tanner*, 1993; *Berresheim et al.*, 2000; *Petäjä et al.*, 2009, *Kürten et al.*, 2011, 2012]. The CIMS measured sulfuric acid at a sampling frequency of 0.1 Hz. Its lower detection limit was estimated to be ~3×10^5 mol cm^{-3} for an integration time of 20 min. The CIMS setup, including the sampling line used at the CLOUD chamber, was calibrated with a calibration system that provided known and stable concentrations of sulfuric acid [*Kürten et al.*, 2012]. The value reported here as sulfuric acid concentration corresponds only to the concentrations of monomer (potentially hydrated) sulfuric acid. The fraction of sulfuric acid in clusters with two or more sulfuric acid molecules is excluded.

SO_2 and O_3 were monitored using standard gas monitors (42i-TLE, Thermo Fisher Scientific Inc., and TEI 49C, Thermo Environmental Instruments, respectively). The water concentration was measured with two dew point

sensors (EdgeTech) used in parallel. One of them had two Peltier elements, whereas the second one had only one Peltier element. To increase their cooling capability and, therefore, increase their potential to measure lower dew/frost temperature, the sensors were placed in the same temperature-controlled rack as the SMPS. The frost/dew point measurements were used in conjunction with temperature measurements to calculate the relative humidity based on equations (7) and (9) from *Murphy and Koop* [2005]. All data reported here refer to relative humidities above liquid water.

2.3. Experimental Particle Formation Rate Evaluation
2.3.1. Experimental Particle Formation Rate at Instrumental Cutoff Size

The particle formation rate J_x is derived from the different particle counters (PSMa, PSMb, DEG-CPCa, DEG-CPCb, and UCPC) at their cutoff size x. Different particle counters have different cutoff sizes that can vary with supersaturation achieved within the instrument, as discussed above in section 2.2.3. J_x is, by definition, the formation rate at which particles grow to the mobility equivalent diameter x (nm), after which they are counted by the CPCs. It is obtained based on the number balance of all particles larger than the cutoff size, $dN_x/dt = J_x - L_x$, which includes both the measured rate of change in the particle counter number concentration that is detected above this measurement threshold, dN_x/dt, and three different loss processes, L_x, which influence the number concentration: coagulation, wall loss, and dilution (growth by condensation is not considered as a loss in this context because the CPC counts all particles larger than the threshold). We calculate J_x using the procedure of *Metzger et al.* [2010],

$$J_x = \frac{dN_x}{dt} + k_{coag}(Dp) \times N_x(Dp)^2 + k_{wall}(Dp) \times N_x(Dp) + k_{dil} \times N_x(Dp), \tag{1}$$

where Dp is the particle diameter and N_x is the number concentration of particles with diameter larger than x nm, as measured by the counter. The dilution rate (k_{dil}) is independent of particle size and equal to $8.94 \times 10^{-5}\,s^{-1}$. It is calculated from the replenishment flow (140 L min^{-1}) divided by the chamber volume (26.1 m^3). The wall loss rate can be approximated by

$$k_{wall}(Dp) = C_{wall} \times (D_v(Dp))^{0.5} \tag{2}$$

where D_v is the diffusion coefficient and C_{wall} is a prefactor equal to 0.0077 cm^{-1}s$^{-0.5}$ for the CLOUD chamber during CLOUD5. C_{wall} was empirically determined with dedicated experiments, by measuring the wall loss rate of sulfuric acid with the CIMS and using the sulfuric acid diffusion coefficient (~0.08 cm^2 s^{-1}). C_{wall} is independent of the vapor if one assumes that there is no reevaporation from the walls. $k_{wall}(Dp)$ is calculated based on the surface-weighted mean diameter of the size distribution. When no size information from the SMPS is available, and for times when the particles are below the cutoff size of the SMPS, k_{wall} is calculated for 6.7 nm particles (the log mean between 3 and 14 nm) to $k_{wall} = 2.2 \times 10^{-4}\,s^{-1}$. This can cause a factor of 2 error in the wall loss rate if all particle diameters are close to either 3 or 14 nm. k_{coag} is approximated using the mean diameter of the size distribution and the diameter (x) of the formed particles. For an experiment at 278 K with 1000 particles per cm^{-3} at a mean size of 5 nm, the values of the three different loss processes referred to by L_x above are 0.0006, 0.347826, and 0.09 cm^{-3} s^{-1} respectively, meaning that wall losses dominate in this case.

Losses due to dilution and wall deposition as particles grow from the critical cluster size to the detection limit of the instruments lead to biases in the CLOUD experiment that will not occur in nature [*Ehrhart and Curtius*, 2013]. However, the state of the art for particle detection that we are using in this study has brought the detection limit close to the critical cluster size (see Table 1), thereby minimizing these effects. Note that all particle sizes (experimental and theoretical) in this paper are reported as mobility equivalent diameter, i.e., geometric diameter plus 0.3 nm [*Tammet*, 1995; *Ku and De La Mora*, 2009]. The measured J_x values are often extrapolated down to a reference mobility diameter (1.7 nm for CLOUD). This extrapolation is uncertain, especially at low-growth rates, because of wall losses and coagulation [*Kürten et al.*, 2015]. In addition, the particle detectors are measuring already near 1.7 nm; therefore, $J_{1.7}$ is not reported for this work. Instead, we use a microphysical model (UHMA2, see section 2.5.2) to predict formation rates at the observational cutoff sizes based on the QC-normalized CNT particle formation rates.

2.4. Experimental Procedure

A new experiment was started only after the chamber temperature, RH, and SO$_2$ and O$_3$ concentrations all reached stable values. The experiment was initiated by opening the aperture between the UV light sources
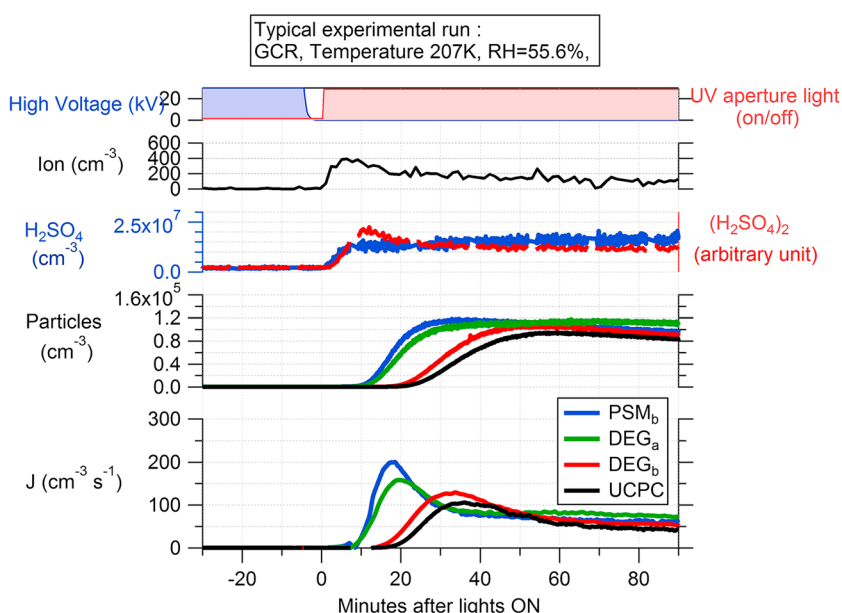
Figure 3. A typical CLOUD run. The first panel shows the clearing field (blue) and UV (red) status, which are the two parameters actively changed to start this run. The second panel shows the negative ion concentration measured by the NAIS. The third panel shows the buildup of the sulfuric acid monomer (blue, left scale, cm^{-3}) and sulfuric acid dimer (red, right scale, arbitrary units) concentrations measured by the CIMS. Particle concentrations measured by various particle counters are shown in the second panel from the bottom, in blue for PSMb, green for DEGa, red for DEGb, and black for UCPC (PSMa was not operational during this run). The particle concentrations measured by all of the counters reached a maximum and then decreased due to an increasing condensation sink inside the chamber. The measured formation rates evaluated with equation (1) at the respective cutoff sizes of these counters are shown in the bottom panel with the same color codes. Counters have different cutoff sizes (see Table 1), and those with lower thresholds detect the rise of particle concentrations earlier and measure a higher formation rate. The formation rates given in Table 2 represent the formation rate plateau for each run.

and the chamber to a predetermined fraction, thereby beginning controlled production of sulfuric acid within the chamber. The sulfuric acid concentration typically reached a steady state within 15 min, corresponding to the inverse of twice the sulfuric acid wall loss time scale. The experiment then continued until observed particle concentrations had increased sufficiently for the particle formation rate to be calculated. A single experimental run typically lasted between 30 min and 3 h. Following the completion of a run, one of two approaches was taken to prepare for the next run. If the condensation sink from the newly formed particles were sufficiently low, one of the parameters could be changed immediately to establish conditions for the next run: either increasing the sulfuric acid concentration by increasing the UV aperture or changing the charging condition inside the chamber. Charging conditions usually went from NEUTRAL to GCR and then to π beam since this sequence increases particle formation rates. In all cases, only one parameter was changed at a time. If the condensation sink was too high (i.e., causing the apparent particle formation rate to be negative and of the same order of magnitude of the expected particle formation rate evaluated by equation (1)), the run was terminated and the chamber was thoroughly flushed to return it to a clean state before establishing the conditions for a new experiment. Following this cleaning, the experimental objectives and multiple parameters were sometimes changed at the cost of a significant time delay between runs.

To illustrate how the CLOUD experiments were performed, a run is shown in Figure 3. It was conducted under the following stable conditions: temperature 207.1 K, relative humidity 55.6%, 44 ppb of SO$_2$, and 1.3 ppm of O$_3$. All of these parameters were kept constant during the run. The run was started by turning off the clearing field (from ±30 kV to 0) to allow ions from galactic cosmic ray ionization to accumulate. Then 4 min later, at time zero, the aperture between the UV light sources and the chamber was switched open, initiating the photochemistry and the buildup of sulfuric acid. Since only 4 min were allowed for ions to accumulate, the ion concentration did not reach its ultimate steady state value for this specific run. The sulfuric acid monomer concentration started to rise as soon as the aperture of the UV lights was switched open, followed very closely by a rise in the sulfuric acid dimer concentration. Within 15 min, sulfuric acid monomers and dimers (as measured

by the CIMS) reached their steady state concentrations in the chamber. The time evolution of particle concentrations measured by four of the five counters is shown in Figure 3. The counters with a lower cutoff threshold detected particles earlier than those with a higher threshold. Note that the lower cutoff threshold counters started to count particles only after the sulfuric acid dimer reached its steady state concentration. This indicates that the lowest size detection limit of the particle counters (transmission and cutoff size) must be higher than the size of hydrated sulfuric acid dimer.

2.5. Theory and Model

2.5.1. QC-Normalized CNT

Full details of the QC-normalized CNT are presented in Paper 1. Briefly, QC-normalized CNT is an extension of work presented in *Noppel et al.* [2002] and *Vehkamaki et al.* [2002] to describe neutral sulfuric acid-water particle formation. The model applies quantum chemistry to solve the partitioning of sulfuric acid into free molecules (whose concentration defines the activity of sulfuric acid vapor) and sulfuric acid hydrates. In the present model, the latest results from electronic-structure calculations [*Kurten et al.*, 2007] are used to determine the sulfuric acid hydrate distribution. The free-energy barrier for nucleation (or its absence) is then determined from the difference between the classical CNT free energy of the critical cluster and the free energy of a reference cluster. The quantum chemically calculated hydrate distribution is also used to derive a reference concentration to which CNT results are normalized in the case of neutral particle formation. In the ion-induced case, the measured ion concentration acts as a reference concentration.

As discussed above, we use the term particle formation to describe the generation of new particles from the vapor phase, in general, and the term nucleation (which in the literature is often used synonymously) only when this process involves surmounting a nucleation free-energy barrier. According to theory, particle formation in the sulfuric acid-water and sulfuric acid-water-ion systems can take place in two ways: (1) through the nucleation regime, where there is a free-energy barrier between the vapor and the liquid phase, and (2) in the kinetic regime, where every molecular collision between two sulfuric acid molecules, or between sulfuric acid and an ion, leads to a freely growing embryo of a new phase. The QC-normalized CNT predicts that both regimes are important, both under the explored experimental conditions and in the atmosphere. In QC-normalized CNT, the ion-induced nucleation rate is proportional to the ion concentration. The maximum ion-induced nucleation rate is equal to the ion production rates, which in this paper are 2 and $20 \, \mathrm{cm}^{-3} \, \mathrm{s}^{-1}$ for GCR and π-beam experiments, respectively. The free input parameters of the QC-normalized CNT are temperature, sulfuric acid concentration, ion concentration, ion production rate, and relative humidity. Their influence on the neutral and ion-induced theoretical particle formation rates with respect to these parameters is illustrated and discussed in Paper 1.

2.5.2. UHMA2: Theoretical Particle Formation Rate Prediction at Instrumental Cutoff Size

The particle formation rate calculated from QC-normalized CNT (J^*_{CNT}) corresponds to the formation rate of particles at the critical cluster size. Formation rates are measured at the instrument cutoff sizes, which are almost always larger than the critical cluster size. In order to compare the measured particle formation rates with predicted formation rates consistently, the rate given by the QC-normalized CNT, J^*_{CNT}, needs to be extrapolated taking into account particle coagulation loss during growth from the critical cluster size to the measurement size. We use a sectional aerosol model (UHMA2) to perform this calculation, starting with J^*_{CNT} to calculate $J^{\mathrm{UHMA2}}_{x, \mathrm{CNT}}$ corresponding to the cutoff size of each of the instruments. For our purposes, this model can simulate the formation rate of any particle size ($J^{\mathrm{UHMA2}}_{x, \mathrm{CNT}}$) by using the following inputs: the formation rate of the critical cluster, the size of the critical cluster, pressure, temperature, and the sulfuric acid concentration. The model includes detailed schemes for condensation [*Nieminen et al.*, 2010] and coagulation. The general dynamic equation was solved with a fourth order Runge-Kutta scheme using an adaptive time step. The model runs were performed with 40 fixed sections distributed logarithmically between the smallest cluster size and 200 nm. For each simulation, the QC-normalized CNT particle formation rate (J^*_{CNT}) and the concentration of sulfuric acid were assumed to be constant in time over the full run, which is a reasonable assumption based on measurement of sulfuric acid concentration inside the CLOUD chamber (see Figure 3). The calculated formation rate at each size (equation (1)) varies strongly at the beginning of the simulation before reaching a stable value. This is due to the continuous change of the condensation sink and coagulation losses for particles between the critical cluster size and the size for which the formation rate is calculated. The predicted steady state formation rate, $J^{\mathrm{UHMA2}}_{x, \mathrm{CNT}}$, is estimated by iterating until the maximum relative change
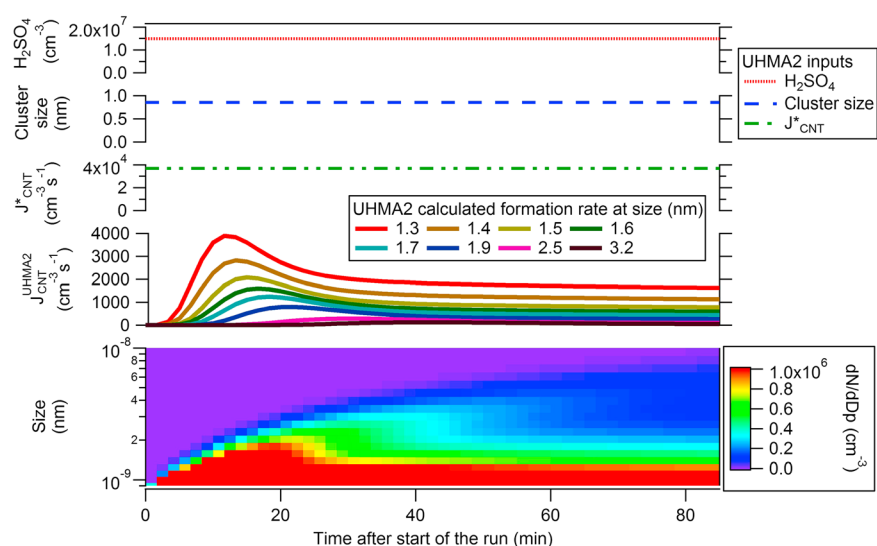
Figure 4. An example of a UHMA2 calculation performed at constant sulfuric acid concentration (1.5×10^7 cm^{-3}), temperature 207 K, a particle formation rate of 37,000 cm^{-3} s^{-1}, and a critical cluster size corresponding to one sulfuric acid molecule. The input parameters are kept constant throughout the run, as seen in the top three panels. The time-dependent UHMA2 calculated formation rates for particle sizes ranging from 1.3 nm to 3.2 nm are shown in the fourth panel. The UHMA2 predicted size distribution of the growing particles is shown in the fifth panel.

between formation rate estimates converges within 1%/h. Figure 4 illustrates a typical UHMA2 calculation for a constant sulfuric acid concentration of 1.5×10^7 cm^{-3} at 207 K. In this simulation, the particle formation rate was 37,000 cm^{-3} s^{-1}; the critical cluster size corresponds to the mobility equivalent diameter of one sulfuric acid molecule, 0.9 nm, i.e., new particle formation is in the kinetic regime. The input parameters were kept constant throughout the simulation. The value of 0.9 nm equivalent mobility diameter for a sulfuric acid molecule in gas was derived from the bulk properties of sulfuric acid and using the equation of *Ku and De La Mora* [2009].

3. Results and Discussion

The measurements of neutral and ion-induced particle formation in the binary sulfuric acid-water system during the CLOUD5 campaign were conducted at five temperatures (207 K, 223 K, 249 K, 279 K, and 299 K). The relative humidity covered the range between 11% and 58%; RH was varied in the low-temperature experiments ($T = 207$–223 K) but kept constant at ~37% RH for the higher temperatures. The sulfuric acid concentration was between 10^5 and 10^9 mol cm^{-3}. Experiments were conducted under three different ionization conditions, namely

1. *NEUTRAL experiments.* Ions were efficiently removed by an external electric field, and the resulting particle formation took place only through the neutral pathway.
2. *GCR experiments.* No clearing field was applied; ions were produced only by galactic cosmic rays. The measured particle formation rate was the sum of neutral and ion-induced rates. The ion concentrations in these experiments had an average value of 308 cm^{-3}.
3. *π-beam experiments.* The π beam produced enhanced ionization by a factor of about 10 compared to that observed under GCR ionization alone. The resulting particle formation rates were the sums of neutral and ion-induced pathways. The ion concentrations in these experiments had an average value of ~3500 cm^{-3} over all temperatures, RHs, and sulfuric acid concentrations.

The particle formation rates were determined according to the activation threshold for each of the UCPC, DEG-CPCs, and PSMs as shown in Table 1. The cutoff size is typically larger than the critical cluster size, and the losses via coagulation and wall losses during cluster growth between those sizes lead to a decreasing formation rate as the cutoff size increases. Table 2 summarizes the experimental conditions, as well as the measured particle formation and growth rates for each of the runs that satisfied the criteria for selection as binary particle formation runs. Due to losses as the particles grow, the highest formation rates should be measured by the particle counter that has the lowest cutoff size; the data generally follow this behavior.

Table 2. Formation Rate Obtained From the CLOUD Experiment for a Set of Temperature, RH, Ions, and Sulfuric Acid Concentration[a]

Experimental Conditions					Measured Formation Rate				
Temperature (K)	Type	Sulfuric Acid (1e6 mol cm^{-3})	RH (%)	Ions (cm^{-3})	J DEGa (# s^{-1} cm^{-3})	J DEGb (# s^{-1} cm^{-3})	J PSMa (# s^{-1} cm^{-3})	J PSMb (# s^{-1} cm^{-3})	J UCPC (# s^{-1} cm^{-3})
205.7 ± 0.0	N	36 ± 22	48.0 ± 0.5	3 ± 6	3.5 ± 1.5		14.6 ± 6.5	4.8 ± 1.8	
205.7 ± 0.0	GCR	38 ± 24	49.1 ± 0.7	58 ± 49	3.1 ± 1.1		10.5 ± 3.7	3.9 ± 1.3	1.2 ± 0.4
206.3 ± 0.1	π beam	48 ± 29	48.9 ± 0.6	973 ± 690	7.4 ± 4.7		13.0 ± 12.0	9.5 ± 5.7	3.7 ± 1.2
206.6 ± 0.0	N	70 ± 45	56.8 ± 1.2	4 ± 7	27.0 ± 9.3	21.3 ± 6.7	20.7 ± 9.6	30.6 ± 13.0	20.3 ± 6.4
206.6 ± 0.0	N	39 ± 24	57.1 ± 0.6	3 ± 9	5.1 ± 2.7	2.7 ± 0.9	13.4 ± 7.3	5.9 ± 2.9	2.4 ± 0.8
206.6 ± 0.0	π beam	44 ± 27	57.3 ± 0.6	1440 ± 900	8.1 ± 4.0	4.7 ± 1.8	14.8 ± 7.4	8.7 ± 4.5	4.2 ± 1.6
206.6 ± 0.0	π beam	84 ± 51	58.4 ± 1.6	665 ± 330	37.1 ± 19.0	31.2 ± 11.0	24.0 ± 11.0	41.9 ± 24.0	30.0 ± 9.3
206.7 ± 0.2	N	19 ± 12	56.9 ± 0.7	5 ± 8	0.3 ± 0.1	0.1 ± 0.1	4.2 ± 1.5	0.3 ± 0.2	0.1 ± 0.1
206.8 ± 0.1	N	72 ± 43	48.3 ± 0.6	3 ± 5	21.4 ± 6.7		18.1 ± 5.8	25.7 ± 8.0	14.4 ± 4.5
206.9 ± 0.1	N	1 ± 1	18.9 ± 0.6	5 ± 10		0.0 ± 0.1			0.0 ± 0.1
206.9 ± 0.1	π beam	120 ± 72	46.6 ± 0.6	1360 ± 680	32.0 ± 11.0	36.5 ± 13.0	18.9 ± 6.0	26.4 ± 9.6	28.6 ± 13.0
206.9 ± 0.0	π beam	75 ± 45	47.5 ± 0.5	1330 ± 670	25.1 ± 12.0		20.3 ± 8.1	28.8 ± 14.0	19.4 ± 6.1
207.1 ± 0.1	N	17 ± 11	16.6 ± 0.6	2 ± 5	0.0 ± 0.1	0.0 ± 0.1	0.2 ± 0.1	0.2 ± 0.1	0.0 ± 0.1
207.2 ± 0.0	GCR	150 ± 92	55.7 ± 0.6	150 ± 120	41.8 ± 14.0	23.9 ± 7.9	19.9 ± 6.4	31.3 ± 11.0	22.7 ± 7.4
207.5 ± 0.1	N	110 ± 69	47.5 ± 0.6	1 ± 2	39.3 ± 13.0		18.9 ± 5.9	39.8 ± 13.0	55.7 ± 18.0
207.8 ± 0.0	π beam	25 ± 16	13.8 ± 0.5	1200 ± 720	0.2 ± 0.1	0.0 ± 0.1	0.7 ± 0.5	1.4 ± 0.6	0.0 ± 0.1
208.2 ± 0.0	GCR	110 ± 67	11.8 ± 0.5	255 ± 160	36.1 ± 12.0		9.4 ± 4.3	62.7 ± 22.0	18.4 ± 6.0
208.2 ± 0.0	N	47 ± 29	12.0 ± 0.5	2 ± 3	1.4 ± 0.5		1.0 ± 1.6	2.7 ± 1.1	0.2 ± 0.2
208.2 ± 0.0	GCR	8 ± 5	12.4 ± 0.5	57 ± 40	0.0 ± 0.1	0.0 ± 0.1	0.0 ± 0.1	0.1 ± 0.1	0.0 ± 0.1
208.2 ± 0.0	N	45 ± 28	12.5 ± 0.5	7 ± 30	1.8 ± 0.6	0.0 ± 0.1	3.9 ± 1.6	7.2 ± 2.3	
208.2 ± 0.0	GCR	45 ± 28	12.5 ± 0.5	231 ± 110	2.2 ± 0.7	0.5 ± 0.2	4.2 ± 1.9	7.9 ± 2.4	0.9 ± 0.3
208.2 ± 0.0	GCR	47 ± 29	12.5 ± 0.5	186 ± 84	2.2 ± 1.7	1.0 ± 0.4	1.7 ± 1.6	5.0 ± 3.6	1.2 ± 0.5
208.2 ± 0.0	π beam	54 ± 33	12.5 ± 0.5	1690 ± 1100	3.7 ± 1.6	1.1 ± 0.4	5.1 ± 2.4	12.5 ± 4.0	1.3 ± 0.6
223.1 ± 0.1	GCR	81 ± 49	48.2 ± 1.2	288 ± 59	4.8 ± 1.7	3.7 ± 1.2	17.8 ± 6.1	7.6 ± 2.6	4.7 ± 1.5
223.4 ± 0.1	N	10 ± 6	11.6 ± 0.5	14 ± 33	0.0 ± 0.1	0.0 ± 0.1	0.0 ± 0.1	0.0 ± 0.1	0.0 ± 0.1
223.4 ± 0.0	N	55 ± 33	48.4 ± 0.6	2 ± 3	0.2 ± 0.2	0.1 ± 0.1	2.6 ± 1.6	0.4 ± 0.3	0.1 ± 0.1
223.5 ± 0.1	GCR	73 ± 44	11.9 ± 0.6	425 ± 190	0.2 ± 0.2		1.6 ± 0.9	0.4 ± 0.2	0.2 ± 0.1
223.5 ± 0.0	N	290 ± 180	12.2 ± 0.5	6 ± 12	41.4 ± 19.0	54.5 ± 19.0	29.4 ± 14.0	55.4 ± 29.0	71.7 ± 24.0
223.5 ± 0.0	N	90 ± 55	26.3 ± 0.6	10 ± 26	1.6 ± 0.7	1.2 ± 0.4	8.8 ± 4.0	3.1 ± 1.2	1.4 ± 0.5
223.5 ± 0.0	π beam	47 ± 29	48.8 ± 0.5	5690 ± 890	0.7 ± 0.9	0.3 ± 0.2	7.0 ± 7.8	1.2 ± 1.1	0.4 ± 0.2
223.5 ± 0.0	π beam	140 ± 83	49.0 ± 0.6	5150 ± 1100	39.5 ± 19.0	27.8 ± 8.5	39.3 ± 22.0	56.5 ± 33.0	44.9 ± 14.0
223.5 ± 0.0	N	79 ± 53	49.3 ± 0.6	9 ± 23	6.4 ± 2.5	6.3 ± 2.0	22.4 ± 9.9	10.6 ± 4.3	6.2 ± 1.9
223.6 ± 0.0	N	68 ± 41	10.9 ± 0.5	13 ± 22	0.0 ± 0.1		0.4 ± 0.2	0.1 ± 0.1	0.0 ± 0.1
223.6 ± 0.0	GCR	290 ± 180	11.2 ± 0.5	294 ± 72	35.4 ± 12.0	48.1 ± 15.0	26.3 ± 8.3	45.6 ± 17.0	60.1 ± 19.0
223.6 ± 0.0	N	130 ± 79	11.3 ± 0.5	14 ± 31	1.0 ± 0.4	1.0 ± 0.3	3.4 ± 1.4	1.6 ± 0.6	0.8 ± 0.5
223.6 ± 0.0	GCR	87 ± 53	24.7 ± 0.5	491 ± 120	1.1 ± 0.4	0.8 ± 0.3	5.9 ± 2.0	1.9 ± 0.7	1.2 ± 0.4
223.6 ± 0.0	GCR	53 ± 32	25.5 ± 0.6	508 ± 130	0.1 ± 0.1	0.0 ± 0.1	1.8 ± 0.8	0.3 ± 0.2	0.1 ± 0.1
223.7 ± 0.0	GCR	120 ± 75	10.6 ± 0.5	305 ± 120	0.9 ± 1.0	0.8 ± 0.3	3.8 ± 3.5	1.4 ± 1.1	0.7 ± 0.3
223.7 ± 0.0	GCR	130 ± 80	23.0 ± 0.5	365 ± 87	6.2 ± 2.1	6.2 ± 1.9	18.7 ± 6.6	10.2 ± 3.5	7.9 ± 2.4
223.7 ± 0.0	N	130 ± 80	23.5 ± 0.5	15 ± 29	6.9 ± 2.3	7.3 ± 2.3	12.0 ± 35.0	9.3 ± 9.9	9.1 ± 2.8
223.7 ± 0.0	N	52 ± 32	25.0 ± 0.7	19 ± 84	0.1 ± 0.1	0.0 ± 0.1	1.0 ± 0.4	0.2 ± 0.1	0.0 ± 0.1
223.8 ± 0.1	N	140 ± 87	51.4 ± 0.7	3 ± 5	45.9 ± 20.0	32.1 ± 14.0	29.5 ± 12.0	39.9 ± 22.0	27.4 ± 8.7
249.0 ± 0.0	N	340 ± 210	26.8 ± 0.5	11 ± 26			0.1 ± 0.1	0.1 ± 0.1	0.1 ± 0.1
249.0 ± 0.0	GCR	360 ± 220	26.8 ± 0.5	292 ± 75			1.4 ± 0.8	0.8 ± 0.4	1.3 ± 0.7
249.0 ± 0.0	GCR	86 ± 53	26.9 ± 0.5	451 ± 110	0.0 ± 0.1	0.0 ± 0.1	0.2 ± 0.1	0.1 ± 0.1	0.0 ± 0.1
249.0 ± 0.0	GCR	170 ± 110	27.0 ± 0.5	465 ± 120			0.9 ± 0.4	0.4 ± 0.2	0.4 ± 0.2
249.0 ± 0.0	N	180 ± 110	27.0 ± 0.5	10 ± 18	0.0 ± 0.1	0.0 ± 0.1	0.1 ± 0.1	0.0 ± 0.1	0.0 ± 0.1
279.3 ± 0.0	π beam	1900 ± 1200	34.0 ± 0.5	6810 ± 1300	13.8 ± 4.4			8.9 ± 8.0	13.4 ± 4.8
279.3 ± 0.0	GCR	1900 ± 1200	37.7 ± 0.5	407 ± 43	2.4 ± 0.8				2.2 ± 0.7
279.3 ± 0.0	GCR	3600 ± 2200	37.7 ± 0.5	263 ± 49	3.5 ± 1.1			2.4 ± 1.1	3.7 ± 1.6
279.4 ± 0.0	π beam	4000 ± 2500	33.9 ± 0.5	4200 ± 340	29.7 ± 9.3	39.0 ± 13.0		37.3 ± 16.0	53.6 ± 18.0
279.4 ± 0.0	π beam	400 ± 240	37.7 ± 0.5	5630 ± 1700				0.3 ± 1.2	0.1 ± 0.1
279.4 ± 0.0	π beam	950 ± 580	37.7 ± 0.5	5460 ± 1900				1.5 ± 2.1	1.8 ± 0.9
279.4 ± 0.0	GCR	960 ± 590	37.7 ± 0.5	361 ± 210					0.2 ± 0.2
279.4 ± 0.0	π beam	1100 ± 640	37.7 ± 0.5	5920 ± 1000				4.7 ± 8.8	3.6 ± 2.8
279.4 ± 0.0	π beam	1700 ± 1100	37.7 ± 0.5	5650 ± 860				8.5 ± 5.9	11.8 ± 3.9
299.3 ± 0.0	GCR	5400 ± 3300	36.0 ± 0.5	242 ± 120	0.0 ± 0.1	0.1 ± 0.1	0.2 ± 0.3	0.0 ± 0.1	0.0 ± 0.1
299.3 ± 0.0	GCR	7700 ± 4700	36.3 ± 0.5	529 ± 140	0.2 ± 0.2	0.4 ± 0.3	0.5 ± 1.4	0.4 ± 0.4	0.2 ± 0.1

[a]The data are sorted by five classes of temperature (207 K, 223 K, 249 K, 279 K, and 299 K), then RH, and then by sulfuric acid concentration.

3.1. Discrimination Between Pure Binary Particle Formation Experiments and Ones in Which Contaminants Introduced Ternary Nucleation

One of the key methods of this study is the use of the APi-TOF-MS in order to distinguish between "pure H_2SO_4/H_2O binary" nucleation and contaminated nucleation, which involves other species than water and sulfuric acid. As previously shown, a few ppt of a third component can influence particle formation processes [*Kirkby et al.*, 2011; *Almeida et al.*, 2013; *Schobesberger et al.*, 2013]. Thus, knowledge of the cluster composition is crucial for studying nucleation processes. Here all measurements are carefully sorted into pure H_2SO_4/H_2O binary or contaminated classes on the basis of molecular identification of the clustered species using the APi-TOF-MS. The contaminated classes found here were sulfuric acid-water-ammonia clusters. Once measured, the "contaminants" become important trace species influencing new particle formation; these ternary particle formation measurements will be the subject of a forthcoming paper. Here we only consider those experiments in which the chemical composition of the system is dominated by clusters composed of only sulfuric acid in the APi-TOF-MS measurements. Although the neutral sulfuric acid dimer can be efficiently stabilized with ammonia [*Hanson and Eisele*, 2002; *Jen et al.*, 2014; *Ortega et al.*, 2012], the charged sulfuric acid dimer and trimer never contain ammonia as they are not stable anions, and rapidly lose ammonia after charging [*Ortega et al.*, 2014]. Thus, only clusters containing at least four sulfuric acid molecules are considered to be good indicators of the presence of ammonia in the clusters ($x \geq 4$). For each experiment, the maximum "purity" ratio between the measured concentration of contaminated clusters (containing x sulfuric acid molecules and 1 ammonia molecule) and the concentration of pure sulfuric acid clusters (containing only *x* sulfuric acid molecules) was evaluated for $4 \leq x \leq 10$. A threshold of 0.05 for the maximum purity ratio was selected to discriminate between the pure H_2SO_4/H_2O binary and contaminated classes; this threshold corresponds roughly to forming 5% of the particles that are produced via ternary mechanisms, with the remainder forming by binary nucleation. One caveat to this method is the possibility that ammonia may be present in the neutral cluster. In our experiments, the charged cluster formation rate includes the neutral pathway through which ammonia might be present but not be detected by the APi-TOF. Ammonia could, therefore, affect the charged particle formation rates (via the neutral pathway) by participating in the stabilization of neutral sulfuric acid-ammonia clusters [*Hanson and Eisele*, 2002; *Jen et al.*, 2014; *Ortega et al.*, 2012]. It should be noted that the water molecules that are inevitably present in the growing clusters are lost before detection in the low-pressure regions of the APi-TOF-MS.

Figure 5 shows two typical negative-mode APi-TOF-MS mass defect spectra observed at 248 K and RH = 38% for pure binary nucleation (purity ratio equal 0) and for ternary nucleation involving NH_3 (purity ratio infinity), respectively, (see *Schobesberger et al.* [2013] for a detailed discussion of mass defect plots). The red points represent molecular clusters that contain only sulfuric acid, whereas the blue points represent clusters containing sulfuric acid and some ammonia. The line formed by the red points represents the clusters containing only sulfuric acid from a monomer to a cluster containing 10 sulfuric acids. The rows of blue dots parallel to the +1 NH_3 arrow correspond to additions of ammonia molecules. All masses that were present in the measured spectrum are shown. For the pure binary nucleation experiment, no charged trace contaminants were observed throughout the nucleation process. In the ternary nucleation experiment, the charged clusters remained ammonia free until they contained four sulfuric acid molecules. Thereafter, the growing clusters took up increasing numbers of ammonia molecules, partially neutralizing the sulfuric acid in the clusters.

Most of the experiments were carried out in a sequence that began with a neutral run, where the APi-TOF-MS is blind, followed by a charged run, where APi-TOF-MS measurements can be used. The only difference between the runs in such a sequence was to turn off of the clearing field and, in some runs, opening the π beam. Care was given to keep the concentrations of trace gases constant in these successive runs; the APi-TOF-MS thus provides some indication of the molecular composition of neutral species after the clearing field is turned off, and ions produced by GCR or π beam can be used to classify the preceding neutral run.

3.2. Experimental Data and QC-Normalized CNT Prediction

We present the observed particle formation rates separately for each temperature and relative humidity. Figures 6–10 correspond to the five values of temperature, with Figures 6 and 7 having separate subfigures for each relative humidity setting. The rates measured by the different instruments are represented by different symbols; estimated 1σ experimental uncertainties are also shown. The dashed lines on the main panels of Figures 6–10 correspond to QC-normalized CNT predicted particle formation rates of the critical cluster,
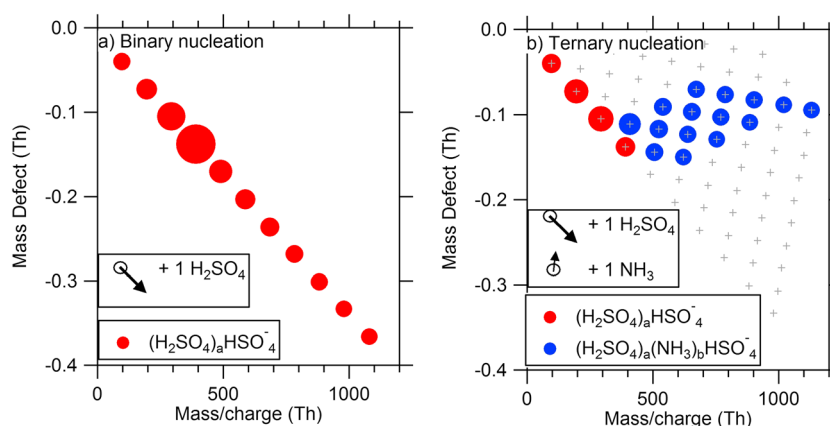
Figure 5. Examples of APi-TOF-MS mass defect spectra in negative mode for (a) pure binary nucleation and (b) ternary nucleation involving NH_3, both measured at 248 K and RH = 38%. The red dots represent molecular clusters composed only of sulfuric acid, whereas the blue dots represent clusters containing sulfuric acid and some ammonia. The size of the dots is proportional to the signal strength from the APi-TOF-MS. The APi-TOF-MS transmission efficiency differs for different masses and is highly dependent on the setting of the APi-TOF-MS. During the CLOUD5 campaigns, the APi-TOF-MS allowed for monitoring masses up to 1200 Th. Grey crosses in Figure 5b represent all possible clusters containing sulfuric acid and ammonia molecules up to 1200 Th. The line formed by the red dots represents the clusters containing only sulfuric acid from a monomer (top left) to a cluster containing 10 sulfuric acids (bottom right). The rows of blue dots parallel to the +1 NH_3 arrow correspond to additions of ammonia molecules. For example, Figure 5b the leftmost blue dot is composed of four sulfuric acid and one ammonia molecule, whereas the rightmost blue dot is composed of 10 sulfuric acids and 9 ammonia molecules. All masses that were present in the measured spectrum are shown. It can clearly be seen that in a pure binary nucleation case, there are no measured trace contaminants involved in the nucleation process. For ion-induced cluster formation in the ternary case, ammonia is taken up after four sulfuric acid molecules have combined into a cluster; the clusters grow further by including more and more ammonia molecules together with sulfuric acid molecules, partially neutralizing the sulfuric acid in the cluster.

J^*_{CNT} (or the kinetic rate if no critical cluster exists); the red line corresponds to neutral formation only, the green line is the sum of neutral and ion-induced formation rates in GCR case, and the blue line is the sum of rates with π beam turned on. The UHMA2 model is used to calculate observed formation rates at the cutoff sizes of the various instruments from the formation rates at the critical cluster size predicted by QC-normalized CNT as explained in section 2.5.2. These (lower) rates, $J^{UHMA2}_{x, CNT}$, are shown using a shaded area with the same color coding as the rates at the critical cluster size. The size of the critical cluster that is predicted by QC-normalized CNT is shown in the upper panels of the figures separately for the neutral and ion-induced cases (red and blue respectively). In the upper panel of each figure, the regimes of nucleation and kinetic particle formation predicted from QC-normalized CNT are marked using full or dashed lines, respectively. For example, in Figure 6a, QC-normalized CNT predicts that ion-induced particle formation is always kinetic, while the neutral pathway switches from nucleation mode to kinetic mode at $2 \times 10^7 \, cm^{-3}$ H_2SO_4 (the diamond symbol). The QC-normalized CNT calculations were performed using the average measured ion concentrations for each temperature.

The measurements and extrapolated theory agree within the instrumental uncertainties at measured cluster sizes. The observed formation rates increase as expected with decreasing temperature (at fixed RH and sulfuric acid concentration), increase with RH (at fixed temperature and sulfuric acid concentration), and are sensitive to charge when there is a free-energy barrier to neutral particle formation. Three domains are clearly visible in the data, consistent with theory: in the nucleation regime the dependence on H_2SO_4 is strong; in the kinetic regime the dependence on H_2SO_4 is weaker; and when ion-induced particle formation is limited by the ion-pair production rate, the dependence on H_2SO_4 vanishes, but the observed rate depends on the ion-pair production rate as expected.

3.2.1. Temperature 207 K and RH = 12% and 50%

The measurements at 207 K, with sulfuric acid concentration varying between 8×10^5 and $2 \times 10^7 \, cm^{-3}$, are presented in Figure 6 for NEUTRAL, GCR, and π-beam cases. The data are split into two different relative humidity ranges, at approximately 12% and 50% RH. The measured particle formation rates show no sensitivity to ion concentrations, as NEUTRAL, GCR, and π-beam measurements all show almost identical formation rates.
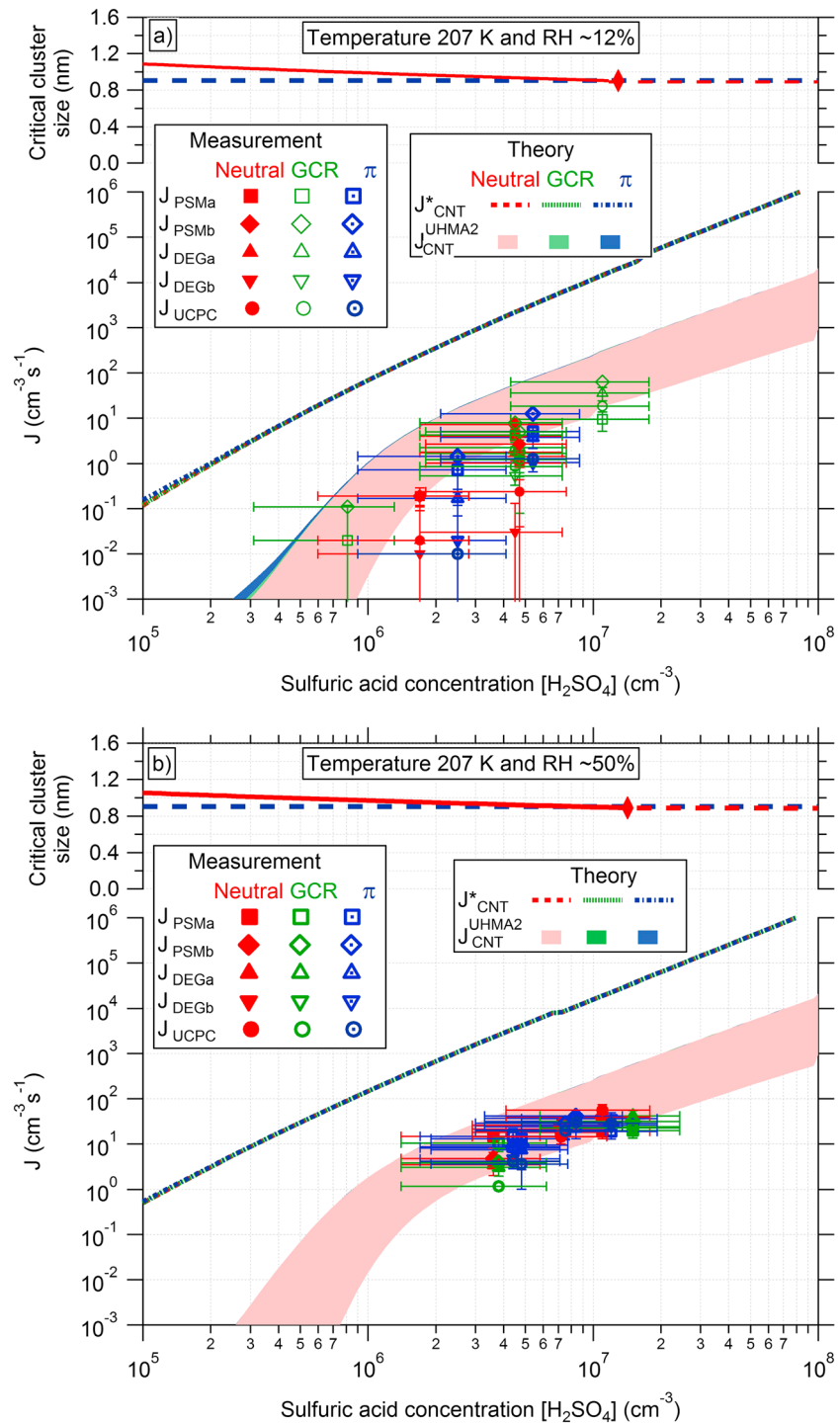
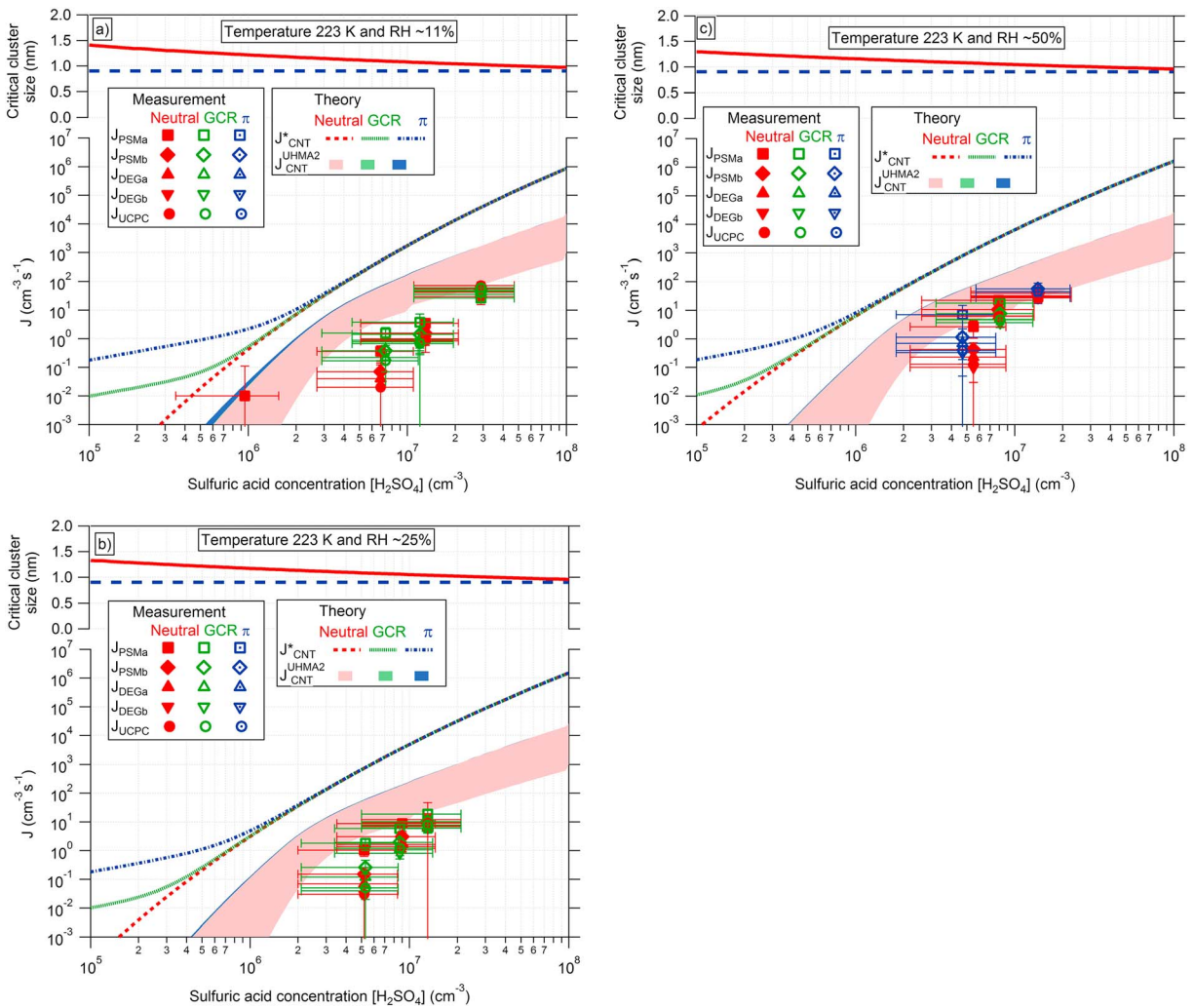**Figure 6.** Binary particle formation rates at 207 K and (a) RH ~ 12% and (b) RH ~ 50%, for NEUTRAL (red), GCR (green), and π (blue) cases. Figure 6a indicates the theoretical neutral (red) and ion-induced (blue) size of the critical cluster, where solid and dashed lines indicate the theoretical nucleation and kinetic particle formation regimes, respectively. The diamond symbol indicates where the regime changes. Figure 6b shows the particle formation rate measured (along with estimated 1σ experimental error bars) by DEGs (triangles), PSMs (squares and diamonds), and UCPC (circle). Dashed lines in Figure 6b show theoretical NEUTRAL (red), GCR (green), and π (blue) particle formation rates calculated at the critical cluster size (in this case, the three-dashed lines are on top of each other). The UHMA2 model is used to extrapolate the formation rates from the critical cluster size predicted by QC-normalized CNT to the formation rates at the cutoff sizes of the various instruments. UHMA2 rates are shown with overlapping shaded bands for NEUTRAL (red), GCR (green), and π (blue) cases. In theoretical calculations, the average ion concentrations were taken to be 150 cm^{-3} in GCR case and 1300 cm^{-3} in π-beam cases.

Figure 7. Binary particle formation rates at 223 K and (a) RH ~ 11%, (b) RH ~ 25%, and (c) RH ~ 50%, for NEUTRAL (red), GCR (green), and π (blue) cases. Colors and symbol coding are the same as in Figure 6. The average GCR and π-beam ion concentrations applied in calculations were 300 cm^{-3} and 5400 cm^{-3}, respectively.

The measurements show a weak dependence on RH, but the experimental uncertainty precludes any definite conclusions. The measurements at low RH show substantially larger uncertainty in the lower bound estimates of the formation rate than those at higher RH. Measured particle formation rates agree within instrumental uncertainties with theoretical rates calculated at the instrumental cutoff sizes. Under these conditions, the theory predicts that ion-induced particle formation is kinetically controlled throughout the measurement range. Moreover, neutral particle formation also proceeds at a rate near the kinetic limit. Thus, as both ion-induced and neutral particle formation are at or near the kinetic regime, and as the sulfuric acid concentration is much higher than the ion concentration, the neutral process dominates the total particle formation rate, and ions do not appreciably affect the new particle formation rate. UHMA2 predictions for theoretical rates are calculated for a range of counter threshold sizes between 1.3 and 3.2 nm. The three theory lines (NEUTRAL, GCR, and π beam) are coincident, and so the shaded areas from the UHMA2 model do also overlap for these three conditions. Extrapolated theoretical formation rates and their dependence on the sulfuric acid concentration match for the first time with experiments within the instrumental uncertainties. Due to the near-kinetic nature of particle formation at this temperature, the theoretical dependence of the rates on RH is weak.

3.2.2. Temperature 223 K and RH 11%, 25%, and 50%

The measurements at 223 K are shown in Figure 7 for RH ~11% (NEUTRAL and GCR), RH ~25% (NEUTRAL and GCR), and RH ~50% (NEUTRAL, GCR, and π beam) for sulfuric acid concentrations in the range 1×10^6 and 3×10^7 cm^{-3}. The data do not show clear evidence of ion enhancement in nucleation rates under these conditions. The
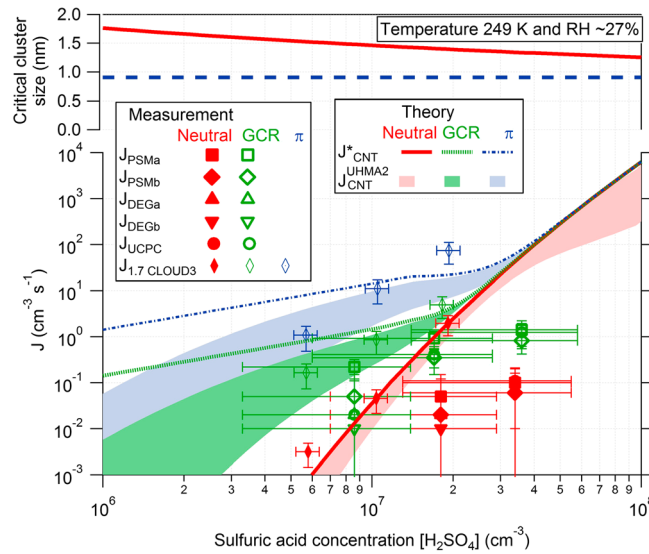
Figure 8. Binary particle formation rates at 249 K, relative humidity of 27% corresponding to CLOUD5 conditions are shown together with CLOUD3 measurements at similar conditions ($T = 248$ K and RH = 38%). The theoretical rates at the two conditions are close to identical. Average ion concentrations are 400 ions cm^{-3} and 4000 cm^{-3} in theoretical calculations for GCR and π-beam cases, respectively. The theory predicts only kinetic ion-induced particle formation at low sulfuric acid concentrations, while neutral nucleation starts producing significant particle formation at sulfuric acid concentrations above 10^7 cm^{-3}. Colors and symbol coding are the same as in Figure 6.
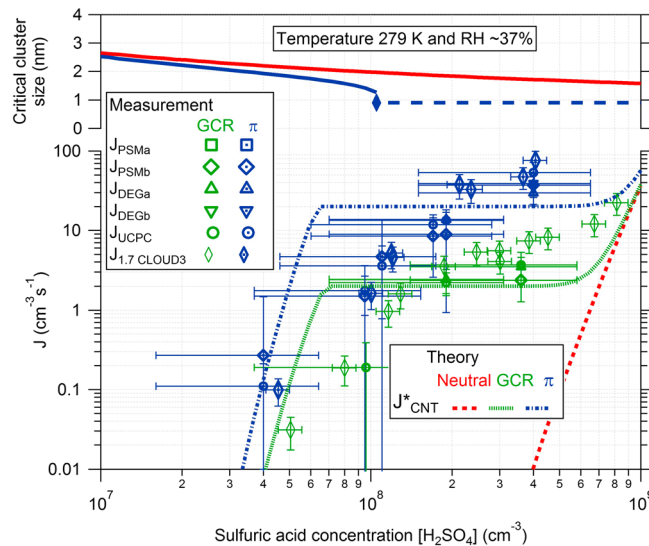
Figure 9. Particle formation rates at 279 K and relative humidity of 37% as measured both during CLOUD3 and CLOUD5. Colors and symbol coding are the same as in Figure 6. For the theoretical GCR calculations, we used the average ion concentration of 340 ions cm^{-3} and an ion-pair production rate (and maximum ion-induced particle formation rate) of 2 ions cm^{-3} s^{-1}. In Pion beam (π) calculations, we used the average ion concentration of 5700 cm^{-3} and an ion-pair production rate (and maximum ion-induced particle formation rate) of 20 cm^{-3} s^{-1}. At this temperature for our data set, $J_{x,\,CNT}^{UHMA2}$ is equal to J_{CNT}^*, due to the large critical cluster size and high sulfuric acid concentration making particles grow fast. Note that the predicted GCR and π formation rates reach plateaus at 2 and 20 cm^{-3} s^{-1}, which correspond to the ion-pair production rates.

measured rates suggest that the particle formation rates are enhanced by roughly a factor 10 when RH increases from 11% to 50%. For this range of the measurements, the relatively steep dependence of observed formation rates on increasing sulfuric acid concentration suggests that particle formation proceeds by a nucleation-type formation process, consistent with theoretical predictions. The theoretical rates obtained using the UHMA2 model overestimate the measured rates by a factor of up to 200 but, in general, capture the observed dependence on sulfuric acid. For a sulfuric acid concentration below 10^6 cm^{-3}, the theory predicts that kinetic ion-induced particle formation dominates over neutral nucleation, though the latter mechanism takes over at higher sulfuric acid concentrations. Under these conditions, the CLOUD5 data do not extend to the region where the nucleation rate is predicted to be enhanced by ions.

3.2.3. Temperature 249 K and RH 27%

Figure 8 shows the measurements at 249 K and at a relative humidity of 27% for the NEUTRAL and GCR cases of sulfuric acid concentrations in the 8×10^6–4×10^7 cm^{-3} range. Observations show a clear enhancement (1 order of magnitude) in particle formation rates due to ions. For this temperature, we have additional NEUTRAL, GCR, and π-beam data of equal quality at RH = 38%, and sulfuric acid concentrations in the 5×10^6-2×10^7 cm^{-3} range from the CLOUD3 campaign in which the experimental approach applied in CLOUD5 was first tested [*Kirkby et al.*, 2011]. The measurements at 248 K reported in *Kirkby et al.* [2011] were made at a mobility diameter of 3.2 nm and then adjusted to 1.7 nm mobility diameter. These adjusted data are also shown in Figure 8. The measured formation rates in the π-beam experiment are 10 times higher than in the GCR experiment. The free ion concentrations in the π-beam experiment were also roughly 10 times higher than in the GCR experiment; the enhancement in the particle formation rate is proportional to the increase in ion concentrations. Neutral particle
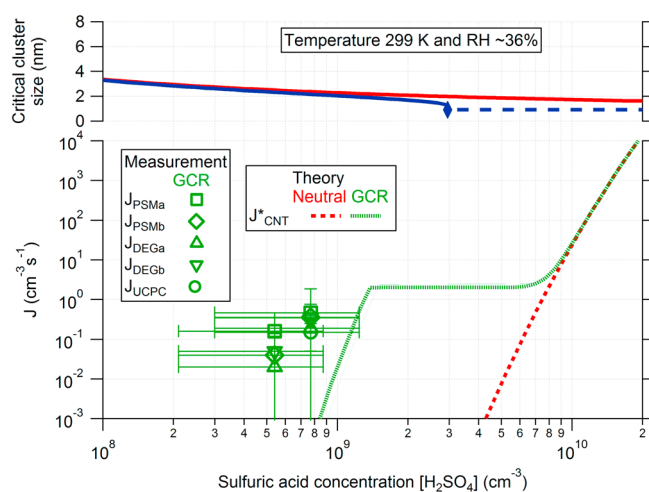
Figure 10. Measured and theoretical nucleation rates at 299 K and relative humidity of 36% at GCR conditions. At this temperature for our data set, $J_{x, CNT}^{UHMA2}$ is equal to J_{CNT}^*, due to the large critical cluster size and high sulfuric acid concentration resulting in fast particle growth. At this temperature, only measurements at two different sulfuric concentrations count as binary within our limitations on the data set. In theoretical calculations, the average ion concentration is 400 ions cm^{-3}, and the ion-pair production rate (and hence maximum ion-induced particle formation rate) is $2 \, cm^{-3} \, s^{-1}$ (level of the plateau).

formation also takes place throughout the measurement range, but ion-induced particle formation dominates.

The theory predicts substantial ion enhancement of particle formation rates in this measurement range, with kinetic ion-induced particle formation reaching the ion production rates (approximated as $2 \, cm^{-3} \, s^{-1}$ and $20 \, cm^{-3} \, s^{-1}$ for GCR and π-beam cases, respectively) at a sulfuric acid concentration of $\sim 10^7 \, cm^{-3}$. The theory also suggests that neutral particle formation takes place through the nucleation event, so that neutral particle formation rates are impeded by the nucleation free-energy barrier at low sulfuric acid concentrations, but exceed the ion-induced particle formation rates at sufficiently high sulfuric acid concentrations.

3.2.4. Temperature 279 K and RH 37%

Measured formation rates at 279 K and relative humidity of 37% are presented in Figure 9 for the combined CLOUD3 and CLOUD5 data. At and above this temperature, traces of NH_3 were frequently found in the CLOUD chamber (see Figure 3 in *Kirkby et al.* [2011]) at levels that may influence the particle formation rate, especially during neutral nucleation. For these reasons, all neutral runs at and above this temperature have been discarded: First, at these higher temperatures, high sulfuric concentrations are required to trigger particle formation. As a result, successive neutral-charge runs could not be performed as cleaning was required between runs to reduce the condensation sink. Thus, as defined in section 3.1, the APi-TOF-MS data could not be used in most of these neutral experiments to distinguish "pure binary"/contaminated nucleation during a neutral run. Second, at these high-temperature experimental conditions, the QC-normalized CNT predicts that binary nucleation is dominated by the ion-induced pathway (see Figures 9 and 10). For example, at a sulfuric acid concentration of $4 \times 10^8 \, cm^{-3}$, the predicted neutral binary nucleation rate is less than $0.01 \, cm^{-3} \, s^{-1}$ compared to ion-induced binary nucleation rates of 2 and $20 \, cm^{-3} \, s^{-1}$, for GCR and π beam, respectively. The ion-induced pathway is even more dominant at lower sulfuric acid concentrations and at higher temperatures. In contrast, as shown in *Kirkby et al.* [2011], the measured neutral ternary formation rates are relatively high under these conditions, so the measured ion-induced ternary formation rates are only a factor 10 higher than the neutral ternary formation rates. Thus, although particle formation in charged runs at these temperatures (where APi-TOF-MS data can be used) is binary (i.e., the ratio of contaminated clusters to pure sulfuric acid clusters is less than 0.05), it is likely that the neutral new particle formation (which cannot be probed with the APi-TOF-MS) is ternary in nature. As discussed above, it is also likely that the charged formation rate measured at these temperatures may be biased via the neutral formation rate pathway where ammonia might be present but not detected. Therefore, data at this and higher temperatures should be taken as an upper limit of the binary formation rate.

For the CLOUD3 data, the measured formation rates show a rapid increase of GCR and π-beam particle formation rates with sulfuric acid concentrations up to the limit where the formation rates equal the ion production rates. The strong dependence on H_2SO_4 suggests that, at this high-temperature, ion-induced particle formation results from nucleation and not from barrier-free kinetic particle formation. The increase in negative ion concentrations (approximately $400 \, cm^{-3}$ for GCR runs and $4000 \, cm^{-3}$ for π-beam runs) increases the formation rates by a factor 10 for π-beam runs; the ion production rates (approximately 2 and 20 ions $cm^{-3} \, s^{-1}$ for GCR and π-beam runs, respectively) satisfactorily explain the saturation of particle formation rates at corresponding values in the measurements (i.e., the ion-induced nucleation rate cannot

be higher than the ion-pair production rate). The nine data points taken during CLOUD5 follow the same trend as does the CLOUD3 data set. The charged particle formation rate increases by about a factor 10 with the similar increase of the ion concentration. Consistent with the observations, the theory predicts that, in this region, ion-induced particle formation proceeds through nucleation. The predicted critical cluster sizes are very close to those at which the formation rates were measured, and the growth rates are fast due to high sulfuric acid concentrations. As a consequence, there is no significant UHMA2 correction to the theoretical cluster formation rate predictions. The theory also predicts that neutral particle formation will not be efficient at the sulfuric acid concentrations studied but will become important at concentration above $10^9 \, cm^{-3}$.

3.2.5. Temperature 299 K and RH 36%

Data at 299 K and relative humidity of 36% are presented in Figure 10. As in the 279 K case, only charged data are presented here. Only experiments at two different sulfuric acid concentrations satisfied the selection criteria; both were at GCR conditions.

While the measurement data are limited, they are consistent with a strong dependence of particle formation on the sulfuric acid concentration. This suggests that particle formation takes place through nucleation instead of kinetic particle formation. Nucleation-type particle formation is also predicted by the theory. Theoretical nucleation rates agree within instrumental uncertainty with the measured rates at $8 \times 10^9 \, cm^{-3}$ sulfuric acid but underestimate the formation rate at lower sulfuric acid concentrations. At this temperature, the theoretical formation rate is strongly dependent on the sulfuric acid concentration; for example, doubling of the sulfuric concentration increases the formation rate by 3 orders of magnitude. It is also likely that the charged formation rate measured at 299 K, like that at 279 K, may be biased via the neutral ternary formation rate pathway. Therefore, these data should be taken as an upper limit of the binary formation rate.

4. Conclusions

We have presented measurements of binary new particle formation for sulfuric acid and water vapor over a range of tropospheric conditions (207–299 K, 11–58% RH, 8×10^5–$10^9 \, cm^{-3}$ H_2SO_4, and ion concentrations between 0 and 6800 ions cm^{-3}) and shown that Quantum Chemistry-normalized Classical Nucleation Theory (QC-normalized CNT) can predict the dependence of binary particle formation rates on temperature, sulfuric acid concentration, relative humidity, ion production rate, and ion concentration, both for neutral and ion-induced particle formation. Our results strongly suggest that the overall picture of particle formation provided by QC-normalized CNT is correct, and that theoretical formation rates can be applied to predict particle formation rates in the binary system over the full range of atmospheric conditions in global modeling, as has been done previously for the neutral binary system [*Merikanto et al.*, 2009].

Interpretation of the experimental results with QC-normalized CNT reveals that (depending on experimental conditions) measured particle formation takes place both in the kinetic regime, where particle formation rates can be derived from molecular collision rates, and in the nucleation regime, where particle formation is impeded by the nucleation free-energy barrier. In the nucleation regime, particle formation rates are strongly dependent on relative humidity. Binary particle formation in the kinetic regime resembles that observed in the boundary layer in that the formation rates are proportional to first and second powers of the sulfuric acid concentration but occurs at temperatures lower than those typically found in the planetary boundary layer. The low temperatures required for pure binary nucleation support the hypothesis that the new particle formation rates observed in the boundary layer require a stabilizing agent, e.g., ammonia, amines, or other species. In the free troposphere, ions can also act as a stabilizer.

Our results support earlier suggestions that binary water-sulfuric acid particle formation can be a major source of new particles in the free troposphere and lower stratosphere, but that it is not typically significant within the boundary layer [*Lovejoy et al.*, 2004; *Kirkby et al.*, 2011]. However, the free troposphere can be a significant source of boundary layer CCN through particle entrainment and a dominant source of CCN in marine environments [*Raes*, 1995; *Merikanto et al.*, 2009]. Therefore, binary water-sulfuric acid particle formation very likely has significant climate relevance. Because binary particle formation occurs via nucleation under most free tropospheric conditions and can therefore be strongly enhanced by stabilizing species, it is still possible that the free-tropospheric process is sometimes enhanced by another species such as ammonia [*Ball et al.*, 1999; *Kirkby et al.*, 2011]. Water-sulfuric acid particle formation is also likely to be the dominant particle formation

process in the stratosphere [*Merikanto et al.*, 2009]. QC-normalized CNT can be combined with global models to study the significance of neutral and ion-induced water-sulfuric acid particle formation in Earth's atmosphere. Another potentially interesting use of the QC-normalized CNT combined with global model is for the study of the atmospheres of other planets, particularly the Venusian atmosphere where water-sulfuric acid particle formation is also likely to be the dominant particle formation process [*Esposito et al.*, 2014].

References

Almeida, J., et al. (2013), Molecular understanding of sulphuric acid-amine particle nucleation in the atmosphere, *Nature*, 502(7471), 359–365, doi:10.1038/nature12663.
Ayers, G. P., R. W. Gillett, and J. L. Gras (1980), On the vapor-pressure of sulfuric-acid, *Geophys. Res. Lett.*, 7(6), 433–436, doi:10.1029/GL007i006p00433.
Ball, S. M., D. R. Hanson, F. L. Eisele, and P. H. McMurry (1999), Laboratory studies of particle nucleation: Initial results for H_2SO_4, H_2O, and NH_3 vapors, *J. Geophys. Res.*, 104(D19), 23,709–23,718, doi:10.1029/1999JD900411.
Benson, D. R., L.-H. Young, F. R. Kameel, and S.-H. Lee (2008), Laboratory-measured nucleation rates of sulfuric acid and water binary homogeneous nucleation from the SO_2^+OH reaction, *Geophys. Res. Lett.*, 35, L11801, doi:10.1029/2008GL033387.
Benson, D. R., J. H. Yu, A. Markovich, and S. H. Lee (2011), Ternary homogeneous nucleation of H_2SO_4, NH_3, and H_2O under conditions relevant to the lower troposphere, *Atmos. Chem. Phys.*, 11(10), 4755–4766, doi:10.5194/acp-11-4755-2011.
Berndt, T., O. Boge, F. Stratmann, J. Heintzenberg, and M. Kulmala (2005), Rapid formation of sulfuric acid particles at near-atmospheric conditions, *Science*, 307(5710), 698–700, doi:10.1126/science.1104054.
Berndt, T., M. Sipila, F. Stratmann, T. Petaja, J. Vanhanen, J. Mikkila, J. Patokoski, R. Taipale, R. L. Mauldin III, and M. Kulmala (2014), Enhancement of atmospheric H_2SO_4/H_2O nucleation: Organic oxidation products versus amines, *Atmos. Chem. Phys.*, 14(2), 751–764, doi:10.5194/acp-14-751-2014.
Berresheim, H., T. Elste, C. Plass-Dulmer, F. L. Eisele, and D. J. Tanner (2000), Chemical ionization mass spectrometer for long-term measurements of atmospheric OH and H_2SO_4, *Int. J. Mass Spectrom.*, 202(1–3), 91–109, doi:10.1016/s1387-3806(00)00233-5.
Bianchi, F., J. Dommen, S. Mathot, and U. Baltensperger (2012), On-line determination of ammonia at low pptv mixing ratios in the CLOUD chamber, *Atmos. Meas. Tech.*, 5(7), 1719–1725, doi:10.5194/amt-5-1719-2012.
Bianchi, F., et al. (2014), Insight into acid-base nucleation experiments by comparison of the chemical composition of positive, negative, and neutral clusters, *Environ. Sci. Technol.*, 48(23), 13,675–13,684, doi:10.1021/es502380b.
Boulaud, D., G. Madelaine, D. Vigla, and J. Bricard (1977), Experimental study on the nucleation of water vapor sulfuric acid binary system, *J. Chem. Phys.*, 66(11), 4854–4860, doi:10.1063/1.433823.
Brus, D., A. P. Hyvarinen, Y. Viisanen, M. Kulmala, and H. Lihavainen (2010), Homogeneous nucleation of sulfuric acid and water mixture: Experimental setup and first results, *Atmos. Chem. Phys.*, 10(6), 2631–2641, doi:10.5194/acp-10-2631-2010.
Brus, D., K. Neitola, A. P. Hyvarinen, T. Petaja, J. Vanhanen, M. Sipila, P. Paasonen, M. Kulmala, and H. Lihavainen (2011), Homogenous nucleation of sulfuric acid and water at close to atmospherically relevant conditions, *Atmos. Chem. Phys.*, 11(11), 5277–5287, doi:10.5194/acp-11-5277-2011.
Cox, R. A. (1973), Some experimental observations of aerosol formation in the photo-oxidation of sulphur dioxide, *J. Aerosol Sci.*, 4(6), 473–483, doi:10.1016/0021-8502(73)90139-0.
Doyle, G. J. (1961), Self nucleation in the sulfuric acid-water system, *J. Chem. Phys.*, 35(3), 795–799, doi:10.1063/1.1701218.
Duplissy, J., et al. (2010), Results from the CERN pilot CLOUD experiment, *Atmos. Chem. Phys.*, 10(4), 1635–1647, doi:10.5194/acp-10-1635-2010.
Ehn, M., et al. (2010), Composition and temporal behavior of ambient ions in the boreal forest, *Atmos. Chem. Phys.*, 10(17), 8513–8530, doi:10.5194/acp-10-8513-2010.
Ehn, M., et al. (2014), A large source of low-volatility secondary organic aerosol, *Nature*, 506(7489), 476–479, doi:10.1038/nature13032.
Ehrhart, S., and J. Curtius (2013), Influence of aerosol lifetime on the interpretation of nucleation experiments with respect to the first nucleation theorem, *Atmos. Chem. Phys.*, 13(22), 11,465–11,471, doi:10.5194/acp-13-11465-2013.
Eisele, F. L., and D. J. Tanner (1993), Measurement of the gas-phase concentration of H_2SO_4 and methane sulfonic-acid and estimates of H_2SO_4 production and loss in the atmosphere, *J. Geophys. Res.*, 98(D5), 9001–9010, doi:10.1029/93JD00031.
Esposito, L. W., A. Colaprete, J. English, R. M. Haberle, and M. A. Kahre (2014), Clouds and aerosols on the terrestrial planets, in *Comparative Climatology of Terrestrial Planets*, pp. 329–353, Univ. of Arizona Press CY, Tucson, Ariz.
Franchin, A., et al. (2015), Experimental investigation of ion-ion recombination at atmospheric conditions, *Atmos. Chem. Phys.*, 15, 7203–7216, doi:10.5194/acp-15-7203-2015.
Friend, J. P., R. A. Barnes, and R. M. Vasta (1980), Nucleation by free-radicals from the photo-oxidation of sulfur-dioxide in air, *J. Chem. Phys.*, 84(19), 2423–2436, doi:10.1021/j100456a018.
Gmitro, J. I., and T. Vermeulen (1964), Vapor-liquid equilibria for aqueous sulfuric acid, *Aiche J.*, 10(5), 740–746, doi:10.1002/aic.690100531.
Gray, L. J., et al. (2010), Solar influences on climate, *Rev. Geophys.*, 48, RG4001, doi:10.1029/2009RG000282.
Hanson, D. R., and F. L. Eisele (2002), Measurement of prenucleation molecular clusters in the NH_3, H_2SO_4, H_2O system, *J. Geophys. Res.*, 107(D12), 4158, doi:10.1029/2001JD001100.
Heist, R. H., and H. Reiss (1974), Hydrates in supersaturated binary sulfuric acid water vapor, *J. Chem. Phys.*, 61(2), 573–581, doi:10.1063/1.1681932.
Iida, K., M. R. Stolzenburg, and P. H. McMurry (2009), Effect of working fluid on sub-2 nm particle detection with a laminar flow ultrafine condensation particle counter, *Aerosol Sci. Technol.*, 43(1), 81–96, doi:10.1080/02786820802488194.
Jaecker-Voirol, A., and P. Mirabel (1988), Nucleation rate in a binary mixture of sulfuric acid and water vapor, *J. Chem. Phys.*, 92(12), 3518–3521, doi:10.1021/j100323a039.
Jen, C. N., P. H. McMurry, and D. R. Hanson (2014), Stabilization of sulfuric acid dimers by ammonia, methylamine, dimethylamine, and trimethylamine, *J. Geophys. Res. Atmos.*, 119, 7502–7514, doi:10.1002/2014JD021592.
Jokinen, T., M. Sipila, H. Junninen, M. Ehn, G. Lonn, J. Hakala, T. Petaja, R. L. Mauldin III, M. Kulmala, and D. R. Worsnop (2012), Atmospheric sulphuric acid and neutral cluster measurements using CI-APi-TOF, *Atmos. Chem. Phys.*, 12(9), 4117–4125, doi:10.5194/acp-12-4117-2012.
Junninen, H., et al. (2010), A high-resolution mass spectrometer to measure atmospheric ion composition, *Atmos. Meas. Tech.*, 3(4), 1039–1053, doi:10.5194/amt-3-1039-2010.
Kangasluoma, J., H. Junninen, K. Lehtipalo, J. Mikkila, J. Vanhanen, M. Attoui, M. Sipila, D. Worsnop, M. Kulmala, and T. Petaja (2013), Remarks on Ion Generation for CPC Detection Efficiency Studies in Sub-3-nm Size Range, *Aerosp. Sci. Technol.*, 47(5), 556–563, doi:10.1080/02786826.2013.773393.

Kiang, C. S., and D. Stauffer (1973), Chemical nucleation theory for various humidities and pollutants, *Faraday Symp. Chem. Soc.*, *7*, 26–33, doi:10.1039/fs9730700026.

Kim, T. O., M. Adachi, K. Okuyama, and J. H. Seinfeld (1997), Experimental measurement of competitive ion-induced and binary homogeneous nucleation in $SO_2/H_2O/N_2$ mixtures, *Aerosol Sci. Technol.*, *26*(6), 527–543, doi:10.1080/02786829708965451.

Kirkby, J. (2007), Cosmic rays and climate, *Surv. Geophys.*, *28*(5–6), 333–375, doi:10.1007/s10712-008-9030-6.

Kirkby, J., et al. (2011), Role of sulphuric acid, ammonia and galactic cosmic rays in atmospheric aerosol nucleation, *Nature*, *476*(7361), 429–U477, doi:10.1038/nature10343.

Ku, B. K., and J. F. de la Mora (2009), Relation between electrical mobility, mass, and size for nanodrops 1–6.5 nm in diameter in air, *Aerosol Sci. Technol.*, *43*(3), 241–249, doi:10.1080/02786820802590510.

Kulmala, M., and A. Laaksonen (1990), Binary nucleation of water sulfuric-acid system—Comparison of classical-theories with different H_2SO_4 saturation vapor-pressures, *J. Chem. Phys.*, *93*(1), 696–701, doi:10.1063/1.459519.

Kulmala, M., M. Lazaridis, A. Laaksonen, and T. Vesala (1991), Extended hydrates interaction-model-hydrate formation and the energetics of binary homogeneous nucleation, *J. Chem. Phys.*, *94*(11), 7411–7413, doi:10.1063/1.460172.

Kulmala, M., A. Toivonen, J. M. Makela, and A. Laaksonen (1998), Analysis of the growth of nucleation mode particles observed in Boreal forest, *Tellus, Ser. B*, *50*(5), 449–462, doi:10.1034/j.1600-0889.1998.t01-4-00004.x.

Kulmala, M., H. Vehkamaki, T. Petaja, M. Dal Maso, A. Lauri, V. M. Kerminen, W. Birmili, and P. H. McMurry (2004), Formation and growth rates of ultrafine atmospheric particles: A review of observations, *J. Aerosol Sci.*, *35*(2), 143–176, doi:10.1016/j.jaerosci.2003.10.003.

Kulmala, M., et al. (2013), Direct observations of atmospheric aerosol nucleation, *Science*, *339*(6122), 943–946, doi:10.1126/science.1227385.

Kupc, A., et al. (2011), A fibre-optic UV system for H_2SO_4 production in aerosol chambers causing minimal thermal effects, *J. Aerosol Sci.*, *42*(8), 532–543, doi:10.1016/j.jaerosci.2011.05.001.

Kürten, A., L. Rondo, S. Ehrhart, and J. Curtius (2011), Performance of a corona ion source for measurement of sulfuric acid by chemical ionization mass spectrometry, *Atmos. Meas. Tech.*, *4*(3), 437–443, doi:10.5194/amt-4-437-2011.

Kürten, A., L. Rondo, S. Ehrhart, and J. Curtius (2012), Calibration of a chemical ionization mass spectrometer for the measurement of gaseous sulfuric acid, *J. Phys. Chem. A*, *116*(24), 6375–6386, doi:10.1021/jp212123n.

Kürten, A., et al. (2014), Neutral molecular cluster formation of sulfuric acid-dimethylamine observed in real time under atmospheric conditions, *Proc. Natl. Acad. Sci. U.S.A.*, *111*(42), 15,019–15,024, doi:10.1073/pnas.1404853111.

Kürten, A., C. Williamson, J. Almeida, J. Kirkby, and J. Curtius (2015), On the derivation of particle nucleation rates from experimental formation rates, *Atmos. Chem. Phys.*, *15*(19), 4063–4075, doi:10.5194/acp-15-4063-2015.

Kurten, T., M. Noppel, H. Vehkamaeki, M. Salonen, and M. Kulmala (2007), Quantum chemical studies of hydrate formation of H_2SO_4 and HSO_4, *Boreal Environ. Res.*, *12*(3), 431–453.

Kurten, T., V. Loukonen, H. Vehkamaki, and M. Kulmala (2008), Amines are likely to enhance neutral and ion-induced sulfuric acid-water nucleation in the atmosphere more effectively than ammonia, *Atmos. Chem. Phys.*, *8*(14), 4095–4103, doi:10.5194/acp-8-4095-2008.

Laakso, L., S. Gagne, T. Petaja, A. Hirsikko, P. P. Aalto, M. Kulmala, and V. M. Kerminen (2007), Detecting charging state of ultra-fine particles: Instrumental development and ambient measurements, *Atmos. Chem. Phys.*, *7*, 1333–1345, doi:10.5194/acp-7-1333-2007.

Lazaridis, M., M. Kulmala, and A. Laaksonen (1991), Binary heterogeneous nucleation of a water sulfuric-acid system—The effect of hydrate interaction, *J. Aerosol Sci.*, *22*(7), 823–830, doi:10.1016/0021-8502(91)90077-u.

Lovejoy, E. R., J. Curtius, and K. D. Froyd (2004), Atmospheric ion-induced nucleation of sulfuric acid and water, *J. Geophys. Res.*, *109*, D08204, doi:10.1029/2003JD004460.

Mäkelä, J. M., V. Jokinen, and M. Kulmala (1995), Small ion mobilities during particle formation from irradiated SO_2 in humid air, *J. Aerosol Sci.*, *26*(Supplement 1(0)), S333–S334, doi:10.1016/0021-8502(95)97074-O.

Manninen, H. E., T. Nieminen, I. Riipinen, T. Yli-Juuti, S. Gagne, E. Asmi, P. P. Aalto, T. Petaja, V. M. Kerminen, and M. Kulmala (2009), Charged and total particle formation and growth rates during EUCAARI 2007 campaign in Hyytiala, *Atmos. Chem. Phys.*, *9*(12), 4077–4089, doi:10.5194/acp-9-4077-2009.

Manninen, H. E., et al. (2010), EUCAARI ion spectrometer measurements at 12 European sites—Analysis of new particle formation events, *Atmos. Chem. Phys.*, *10*(16), 7907–7927, doi:10.5194/acp-10-7907-2010.

Marti, J. J., A. Jefferson, X. P. Cai, C. Richert, P. H. McMurry, and F. Eisele (1997), H_2SO_4 vapor pressure of sulfuric acid and ammonium sulfate solutions, *J. Geophys. Res.*, *102*(D3), 3725–3735, doi:10.1029/96JD03064.

Megaw, W. J., and R. D. Wiffen (1961), The generation of condensation nuclei by ionising radiation, *Geogr. Ann., Ser. A*, *50*(1), 118–128, doi:10.1007/bf02000635.

Merikanto, J., D. V. Spracklen, G. W. Mann, S. J. Pickering, and K. S. Carslaw (2009), Impact of nucleation on global CCN, *Atmos. Chem. Phys.*, *9*(21), 8601–8616, doi:10.5194/acp-9-8601-2009.

Merikanto, J., J. Duplissy, A. Määttänen, H. Henschel, N. M. Donahue, D. Brus, S. Schobesberger, M. Kulmala, and H. Vehkamäki (2016), Effect of ions on sulfuric acid-water binary particle formation: 1. Theory for kinetic- and nucleation-type particle formation and atmospheric implications, *J. Geophys. Res. Atmos.*, *121*, doi:10.1002/2015JD023538.

Metnieks, A. L., and L. W. Pollak (1959), Instructions for use of photo-electric condensation nucleus counters, their care and maintenance together with calibration and auxiliary tables, *School of Cosmic Physics Dublin Inst. for Advanced Studies, Ireland*, *16*.

Metzger, A., et al. (2010), Evidence for the role of organics in aerosol particle formation under atmospheric conditions, *Proc. Natl. Acad. Sci. U.S.A.*, *107*(15), 6646–6651, doi:10.1073/pnas.0911330107.

Mirabel, P., and J. L. Clavelin (1978), Experimental-study of nucleation in binary-mixtures—Nitric acid water and sulfuric acid water systems, *J. Chem. Phys.*, *68*(11), 5020–5027, doi:10.1063/1.435617.

Mirabel, P., and J. L. Katz (1974), Binary homogeneous nucleation as a mechanism for formation of aerosols, *J. Chem. Phys.*, *60*(3), 1138–1144, doi:10.1063/1.1681124.

Mizin, S. V., V. S. Makhmutov, O. S. Maksumov, and A. N. Kvashnin (2011), Application of multithreading programming to physical experiment, *Bull. Lebedev Phys. Inst.*, *38*(2), 34–40, doi:10.3103/s1068335611020023.

Murphy, D. M., and T. Koop (2005), Review of the vapour pressures of ice and supercooled water for atmospheric applications, *Q. J. R. Meteorol. Soc.*, *131*(608), 1539–1565, doi:10.1256/qj.04.94.

Murphy, S. M., A. Sorooshian, J. H. Kroll, N. L. Ng, P. Chhabra, C. Tong, J. D. Surratt, E. Knipping, R. C. Flagan, and J. H. Seinfeld (2007), Secondary aerosol formation from atmospheric reactions of aliphatic amines, *Atmos. Chem. Phys.*, *7*(9), 2313–2337, doi:10.5194/acp-7-2313-2007.

Nieminen, T., K. E. J. Lehtinen, and M. Kulmala (2010), Sub-10 nm particle growth by vapor condensation—Effects of vapor molecule size and particle thermal speed, *Atmos. Chem. Phys.*, *10*(20), 9773–9779, doi:10.5194/acp-10-9773-2010.

Noppel, M., H. Vehkamaki, and M. Kulmala (2002), An improved model for hydrate formation in sulfuric acid-water nucleation, *J. Chem. Phys.*, *116*(1), 218–228, doi:10.1063/1.1423333.

O'Dowd, C. D., P. P. Aalto, Y. J. Yoon, and K. Hameri (2004), The use of the pulse height analyser ultrafine condensation particle counter (PHA-UCPC) technique applied to sizing of nucleation mode particles of differing chemical composition, *J. Aerosol Sci.*, *35*(2), 205–216, doi:10.1016/j.jaerosci.2003.08.003.

Ortega, I. K., O. Kupiainen, T. Kurtén, T. Olenius, O. Wilkman, M. J. McGrath, V. Loukonen, and H. Vehkamäki (2012), From quantum chemical formation free energies to evaporation rates, *Atmos. Chem. Phys.*, *12*(1), 225–235, doi:10.5194/acp-12-225-2012.

Ortega, I. K., T. Olenius, O. Kupiainen-Määttä, V. Loukonen, T. Kurtén, and H. Vehkamäki (2014), Electrical charging changes the composition of sulfuric acid-ammonia/dimethylamine clusters, *Atmos. Chem. Phys.*, *14*(15), 7995–8007, doi:10.5194/acp-14-7995-2014.

Petäjä, T., R. L. Mauldin, E. Kosciuch, J. McGrath, T. Nieminen, P. Paasonen, M. Boy, A. Adamov, T. Kotiaho and M. Kulmala (2009), Sulfuric acid and OH concentrations in a boreal forest site, *Atmos. Chem. Phys.*, *9*(19), 7435–7448, doi:10.5194/acp-9-7435-2009.

Praplan, A. P., F. Bianchi, J. Dommen, and U. Baltensperger (2012), Dimethylamine and ammonia measurements with ion chromatography during the CLOUD4 campaign, *Atmos. Meas. Tech.*, *5*(9), 2161–2167, doi:10.5194/amt-5-2161-2012.

Raes, F. (1995), Entrainment of free tropospheric aerosols as a regulating mechanism for cloud condensation nuclei in the remote marine boundary-layer, *J. Geophys. Res.*, *100*(D2), 2893–2903, doi:10.1029/94JD02832.

Raes, F., and A. Janssens (1986), Ion-induced aerosol formation in a $H_2O-H_2SO_4$ system: 2. Numerical-calculations and conclusions, *J. Aerosol Sci.*, *17*(4), 715–722, doi:10.1016/0021-8502(86)90051-0.

Raes, F., A. Janssens, and G. Eggermont (1985), A synergism between ultraviolet and gamma-radiation in producing aerosol-particles from $SO_2-H_2SO_4$ laden atmospheres, *Atmos. Environ.*, *19*(7), 1069–1073, doi:10.1016/0004-6981(85)90191-x.

Reiss, H. (1950), The kinetics of phase transitions in binary systems, *J. Chem. Phys.*, *18*(6), 840–848, doi:10.1063/1.1747784.

Reiss, H., D. I. Margolese, and F. J. Schelling (1976), Experimental-study of nucleation in vapor mixtures of sulfuric-acid and water, *J. Colloid Interface Sci.*, *56*(3), 511–526, doi:10.1016/0021-9797(76)90118-1.

Riccobono, F., et al. (2012), Contribution of sulfuric acid and oxidized organic compounds to particle formation and growth, *Atmos. Chem. Phys.*, *12*(20), 9427–9439, doi:10.5194/acp-12-9427-2012.

Riccobono, F., et al. (2014), Oxidation products of biogenic emissions contribute to nucleation of atmospheric particles, *Science*, *344*(6185), 717–721, doi:10.1126/science.1243527.

Roedel, W. (1979), Measurement of sulfuric-acid saturation vapor-pressure–Implications for aerosol formation by heteromolecular nucleation, *J. Aerosol Sci.*, *10*(4), 375–386, doi:10.1016/0021-8502(79)90032-6.

Schnitzhofer, R., et al. (2014), Characterisation of organic contaminants in the CLOUD chamber at CERN, *Atmos. Meas. Tech.*, *7*(7), 2159–2168, doi:10.5194/amt-7-2159-2014.

Schobesberger, S., et al. (2013), Molecular understanding of atmospheric particle formation from sulfuric acid and large oxidized organic molecules, *Proc. Natl. Acad. Sci. U.S.A.*, *110*(43), 17,223–17,228, doi:10.1073/pnas.1306973110.

Schobesberger, S., et al. (2015), On the composition of ammonia-sulfuric-acid ion clusters during aerosol particle formation, *Atmos. Chem. Phys.*, *15*(1), 55–78, doi:10.5194/acp-15-55-2015.

Shugard, W. J., and H. Reiss (1976), Transient nucleation in $H_2O-H_2SO_4$ mixtures—Stochastic approach, *J. Chem. Phys.*, *65*(7), 2827–2840, doi:10.1063/1.433432.

Shugard, W. J., R. H. Heist and H. Reiss (1974), Theory of vapor-phase nucleation in binary-mixtures of water and sulfuric-acid, *J. Chem. Phys.*, *61*(12), 5298–5305, doi:10.1063/1.1681879.

Sipila, M., et al. (2010), The role of sulfuric acid in atmospheric nucleation, *Science*, *327*(5970), 1243–1246, doi:10.1126/science.1180315.

Stolzenburg, M. R., and P. H. McMurry (1991), An ultrafine aerosol condensation nucleus counter, *Aerosol Sci. Technol.*, *14*(1), 48–65, doi:10.1080/02786829108959470.

Svensmark, H., J. O. P. Pedersen, N. D. Marsh, M. B. Enghoff, and U. I. Uggerhoj (2007), Experimental evidence for the role of ions in particle nucleation under atmospheric conditions, *Proc. R. Soc. A*, *463*(2078), 385–396, doi:10.1098/rspa.2006.1773.

Tammet, H. (1995), Size and mobility of nanometer particles, clusters and ions, *J. Aerosol Sci.*, *26*(3), 459–475, doi:10.1016/0021-8502(94)00121-E.

Vanhanen, J., J. Mikkila, K. Lehtipalo, M. Sipila, H. E. Manninen, E. Siivola, T. Petaja, and M. Kulmala (2011), Particle size magnifier for nano-CN detection, *Aerosol Sci. Technol.*, *45*(4), 533–542, doi:10.1080/02786826.2010.547889.

Vehkamaki, H., M. Kulmala, I. Napari, K. E. J. Lehtinen, C. Timmreck, M. Noppel, and A. Laaksonen (2002), An improved parameterization for sulfuric acid-water nucleation rates for tropospheric and stratospheric conditions, *J. Geophys. Res.*, *107*(D22), 4622, doi:10.1029/2002JD002184.

Viisanen, Y., M. Kulmala, and A. Laaksonen (1997), Experiments on gas-liquid nucleation of sulfuric acid and water, *J. Chem. Phys.*, *107*(3), 920–926, doi:10.1063/1.474445.

Vohra, K. G., M. C. S. Ramu and T. S. Muraleedharan (1984), An experimental-study of the role of radon and its daughter products in the conversion of sulfur-dioxide into aerosol-particles in the atmosphere, *Atmos. Environ.*, *18*(8), 1653–1656, doi:10.1016/0004-6981(84)90387-1.

Voigtlaeander, J., J. Duplissy, L. Rondo, A. Kuerten, and F. Stratmann (2012), Numerical simulations of mixing conditions and aerosol dynamics in the CERN CLOUD chamber, *Atmos. Chem. Phys.*, *12*(4), 2205–2214, doi:10.5194/acp-12-2205-2012.

Wilemski, G. (1987), Revised classical binary nucleation theory for aqueous alcohol and acetone vapors, *J. Phys. Chem.*, *91*(10), 2492–2498, doi:10.1021/j100294a011.

Wilson, C. T. R. (1895), The effect of Rontgen's rays on cloudy condensation, *Proc. R. Soc. Lond.*, *59*, 338–339.

Wilson, C. T. R. (1899), On the condensation nuclei produced in gases by the action of Rontgen rays, uranium rays, ultra-violet light and other agents, *Philos. Trans. R. Soc. London, Ser. A*, *192*, 403–453.

Wimmer, D., et al. (2013), Performance of diethylene glycol-based particle counters in the sub-3 nm size range, *Atmos. Meas. Tech.*, *6*(7), 1793–1804, doi:10.5194/amt-6-1793-2013.

Wimmer, D., et al. (2015), Technical Note: Using DEG-CPCs at upper tropospheric temperatures, *Atmos. Chem. Phys.*, *15*, 7547–7555, doi:10.5194/acp-15-7547-2015.

Wyslouzil, B. E., J. H. Seinfeld, R. C. Flagan, and K. Okuyama (1991), Binary nucleation in acid water-systems: 2. Sulfuric-acid water and a comparison with methanesulfonic-acid water, *J. Chem. Phys.*, *94*(10), 6842–6850, doi:10.1063/1.460262.

Young, L. H., D. R. Benson, F. R. Kameel, J. R. Pierce, H. Junninen, M. Kulmala, and S. H. Lee (2008), Laboratory studies of H_2SO_4/H_2O binary homogeneous nucleation from the SO_2+OH reaction: Evaluation of the experimental setup and preliminary results, *Atmos. Chem. Phys.*, *8*(16), 4997–5016, doi:10.5194/acp-8-4997-2008.

Zhao, J., F. L. Eisele, M. Titcombe, C. G. Kuang, and P. H. McMurry (2010), Chemical ionization mass spectrometric measurements of atmospheric neutral clusters using the cluster-CIMS, *J. Geophys. Res.*, *115*, 16, doi:10.1029/2009JD012606.

Zhang, R., L. Wang, A. F. Khalizov, J. Zhao, J. Zheng, R. L. McGraw, and L. T. Molina (2009), Formation of nanoparticles of blue haze enhanced by anthropogenic pollution, *Proc. Natl. Acad. Sci. U.S.A.*, *106*(42), 17,650–17,654, doi:10.1073/pnas.0910125106.

Zhang, R., A. Khalizov, L. Wang, M. Hu, and W. Xu (2012), Nucleation and growth of nanoparticles in the atmosphere, *Chem. Rev.*, *112*(3), 1957–2011, doi:10.1021/cr2001756.

Zhang, R. Y., I. Suh, J. Zhao, D. Zhang, E. C. Fortner, X. X. Tie, L. T. Molina, and M. J. Molina (2004), Atmospheric new particle formation enhanced by organic acids, *Science*, *304*(5676), 1487–1490, doi:10.1126/science.1095139.

Ziereis, H., and F. Arnold (1986), Gaseous ammonia and ammonium-ions in the free troposphere, *Nature*, *321*(6069), 503–505, doi:10.1038/321503a0.

Zollner, J. H., W. A. Glasoe, B. Panta, K. K. Carlson, P. H. McMurry, and D. R. Hanson (2012), Sulfuric acid nucleation: Power dependencies, variation with relative humidity, and effect of bases, *Atmos. Chem. Phys.*, *12*(10), 4399–4411, doi:10.5194/acp-12-4399-2012.